LUND UNIVERSITY

LTH
FACULTY OF ENGINEERING

Continuous Quantum Control of Quantum Dot Systems

Daniel Holst

Thesis submitted for the degree of Master of Science
Project duration: 4 months (30 ECTS)

Supervised by Peter Samuelsson & Björn Annby-Andersson

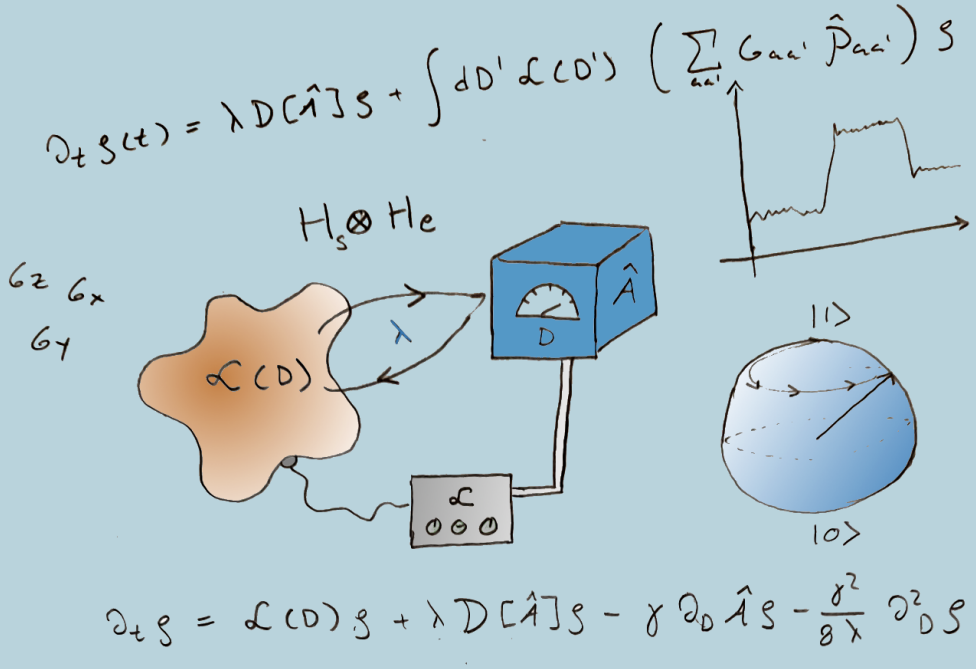

Department of Physics
Division of Mathematical Physics
December 2022

Populärvetenskaplig sammanfattning

Kontroll och återkoppling är något vi alla förlitar oss på varje dag, vi litar på att busschaufförен observerar vägförhållandena och återkopplar informationen genom att utföra korrekta kursändringar, vi är alla tacksamma att termostaten på elementet justerar rumstemperaturen givet omgivningens tillstånd, vilket också är ett enkelt exempel på kontroll-återkopplings loopen. Mängden tillämpningar av kontrollteori är idag nästintill oräkneliga med tillämpningar inom så vitt skilda ämnen som aktiemarknaden och telekommunikation. Men genom teknikens konstanta frammarsch har det idag växt fram nya typer av system i behov av kontroll och styrning, system som skiljer sig något från vad vi i vår vardagliga ”klassiska” värld har vana utav, nämligen kvantmekaniska system.

Kvantmekaniken är en teori som växte fram under början av 1900 för att förklara nya observationer som tycktes strida mot vad den klassiska fysiken förutsade, kvantmekaniken visade sig kunna förklara dessa nya observationer med häpnadsväckande precision men tvingade även på oss nya begrepp såsom superposition, osäkerhetsprincipen och vågfunktionens-kollaps, några begrepp som får de flesta fysiker att klia sig i huvudet mer ofta en vad hen skulle vilja. Kvantmekaniken brukar beskrivas som teorin för den mikroskopiska världen men är fundamentalt en teori som gäller för all materia i universum. Teorin studeras dock enklast på mycket små system eftersom dessa kvantmekaniska effekter enkelt störs ut genom interaktion med omgivningen, något som kallas för dekoherens, vilket även förklarar varför vi i vårt vardagliga makroskopiska universum inte observerar våra katter som vågfunktionen och varför den klassiska fysiken (som en första approximation) gäller i de flesta fallen.

I takt med att tekniken blir mindre och mindre är dessa effekter dock inte längre något man kan ignorera, nu handlar det snarare om att se huruvida man kan använda de spännande effekterna som beskrivs utav kvantmekaniken till sin fördel. Ett populärt förslag till detta är så kallade kvantdatorer som använder superposition av sina beräkningsenheter (s.k. qubits - Quantum Bits) för att utföra vissa beräkningar snabbare än vad någon klassisk dator kan. Superposition innebär att en bit kan vara både 0 och 1 samtidigt samt alla möjliga kombinationer däremellan. Genom att sedan låta dessa bitar samverka på särskilt kontrollerade sätt kan man visa att en sådan dator teoretiskt kan utföra särskilda uppgifter otroligt snabbt. Ett av de största problemen man stöter på när man ska designa en sådan dator är hur man ska kunna minimera störningar från omgivningen för att behålla de kvantmekaniska effekterna samtidigt som man fortfarande ska kunna styra qubitsen för att utföra beräkningarna man är ute efter. Här är förhoppningen att implementering av kontroll och återkoppling ska kunna lösa dessa problem.

Vid kontroll av kvantmekaniska system stöter man dock på lite oväntad patrull. En av kvantmekanikens märkliga förutsägelser är nämligen att systemet och mätinstrumentet inte är frånkopplade från varandra, en mätning på en kvantsystem kommer påverka tillståndet av systemet. För att kunna mäta tillståndet av systemet för att sedan använda denna informationen till att kontrollera systemet, måste vi alltså nödvändigtvis störa systemet och därmed påverka dess tillstånd, denna växelverkan mellan mätning och system kallas för back-action. För att undvika back-action men fortfarande kunna styra kvantsystem har man därför konstruerat något som kallas för svaga mätningar. Svaga mätningar extraherar bara en liten mängd information från systemet och stör därför inte systemet så mycket. Priset vi får betala är att vi kanske inte nödvändigtvis kommer utföra korrekt återkoppling givet den inkompletta informationen av systemets tillstånd.

Björn Annby-Andersson et.al. publicerade nyligen en ny typ av ekvation som gör det möjligt att beskriva ett kvantmekaniskt system som kontrolleras genom att utföra svaga mätningar. Liknande ekvationer har tidigare publicerats men har (bortsett från några specialfall) krävt datorer för att kunna lösas. Det som är spännande med denna nya ekvationen är att det gör det möjligt att räkna ut effekter av styrning för dessa system för hand med penna och papper för en mycket större klass av återkopplings-situationer en vad som tidigare varit möjligt.

Denna masterupsats har undersökt denna nya ekvation och applicerat den på två olika testsystem bestående av två olika kvantmekaniska komponenter (kvantprickar) för att se hur transportprocesserna i dessa system påverkas av styrningen och den svaga mätprocessen. Den har även studerat huruvida det är möjligt att implementera något som kallas för Maxwell demoner i dessa system.

En Maxwell Demon är en hypotetisk varelse som figurerar i tankeexperiment från den klassiska fysiken. Tanke-experimenten har förbryllat många generationer av fysiker eftersom de till synes verkar visa att det går att bryta mot en av fysikens huvudprinciper nämligen att o-ordningen av ett system alltid ökar, fysiker kvantifierar detta genom begreppet entropi som beskriver hur väl utfördelad energi är inom ett system. Att bryta mot denna principen skulle kunna vara att få värme att vandra från ett kallt bad till ett varmt bad eller få partiklar att röra sig från låg koncentration till hög koncentration, helt enkelt att gå emot vad som spontant skulle ske. Dessa processer skulle vanligtvis kräva att man tillför energi till systemet.

Det visar sig dock i dessa tankeexperiment att man genom att implementera en observatör (denna observatörer är vad som med lite glimt i ögat benämnts som en demon) som genom att observera ett system och utföra operationer som inte kräver att extra energi tillsätts till systemet kan få just dessa processer att uppstå. Alltså få värme att vandra från ett kallt bad till ett varmt eller få partiklar att röra sig mot högre koncentration.

Lösningen på paradoxen är att för att demonen ska kunna utföra sina observationer och sedan använda den infångande informationen måste skapa precis tillräckligt med o-ordning (positiv entropi) för att kompensera för den tillsynes olagliga ordningen. Detta har mycket intressanta konsekvenser, det visar sig nämligen att man kan formulera denna process som att demonen konverterar information till energi. Nyligen har det blivit möjligt att tillverka nanometer-stora system i labbet för att undersöka denna typen av process, detta arbete utgör därmed en teoretisk förstudie för kommande experiment.

Abstract
Control and feedback operation of quantum systems have in recent years gained alot of interest since they are fundamental to achieving functional quantum information processing systems but also of great importance in applications of information to energy conversion within quantum thermodynamics. This thesis has treated a new formalism for feedback control of quantum systems. This formalism is able to analytically describe non-linear feedback protocols, something that was previously described by stochastic equations, only solvable numerically. This new formalism was applied to two test systems, one classical system as well as one quantum system consisting of double dots. These systems were studied using both analytical and full numerical solutions. It was found that by using non-linear feedback schemes both these systems could be operated as information engines.

Acknowledgements
I would like to extend my warmest thanks to my supervisors Peter Samuelsson and Björn Annby-Andersson for their excellent guidance and support during the project. I would also like to thank Faraj Bakhshinezhad and Patrick Potts for their invaluable input during the project. Finally I would like to thank my friends and family for their love and support throughout the process of completing this thesis.

”If you think you understand quantum mechanics, you don’t understand quantum mechanics.” - R.P. Feynman

Contents

1 Introduction **3**

2 Theory **5**
2.1 Maxwell's Demon & Information Engines . . . 5
2.2 Density matrices & Master equations . . . 6
2.3 Generalized Quantum Measurements (POVM'S) . . . 7
2.4 Feedback signal . . . 8
2.5 Derivation of Formalism: Part I . . . 9
2.6 Derivation of Formalism: Part II . . . 10
2.7 Separation of Timescales . . . 11
2.8 Full Counting Statistics . . . 13
2.8.1 Cumulant expansion . . . 15
2.9 Numerical Approach . . . 16

3 Classical system - Single Electron Transistor (S.E.T.) **18**
3.1 Model & Feedback scheme . . . 18
3.2 Applying Separation of Timescales . . . 20
3.3 S.E.T with counting field . . . 21
3.4 Analytical Results . . . 22
3.5 Numerics . . . 24
3.6 Numerics Results . . . 24

4 Quantum system - Double Dot **30**
4.1 Model & Feedback scheme . . . 30
4.2 Topological Error . . . 34
4.3 Applying Separation of Timescales . . . 36
4.3.1 Sanity check - Overall Transport . . . 38
4.3.2 More sanity checks - No control . . . 39
4.3.3 Ideal D_1 detector limit . . . 39
4.3.4 Some other limits of interest . . . 40
4.3.5 Power production considerations . . . 40
4.4 Analytical Results . . . 42
4.5 Numerics . . . 45
4.6 Numerics Results . . . 45

5 Conclusions & Outlook **51**

6 Appendix **53**
6.1 Proof of useful expressions . . . 53
6.1.1 Identity 1 . . . 53

6.1.2 Identity 2 53
6.2 Details of Numerics 53
6.2.1 SET system 53
6.2.2 Quantum Double Dot 54

Chapter 1

Introduction

The field of Quantum information have had an explosion in activity since Peter Shor, in 1994, published his now famous article "Algorithms for quantum computation: discrete logarithms and factoring" [1], in which he showed that a hypothetical quantum computer could be used to effectively solve the prime factorization problem. However, constructing a useful quantum computer has proved to be a tremendous technological and theoretical challenge. The crux of the problem is how to limit and account for decoherence of the qubit states of the computer. To meet this challenge, a large number of different approaches and methods have been developed to tackle the problem of efficiently monitoring and controlling qubit states while at the same time minimizing the influence of dephasing. However, the overall problem of controlling quantum systems through measurement and feedback and the questions related to this problem have today grown into its on field of study, grouped together under the umbrella term quantum control. This type of control clearly have many applications within quantum computing and quantum information processing today but started out within the field of quantum optics [2]. Here one of the more important applications of quantum control is also to suppress the effect of environmental noise, which leads to dechoerence in quantum systems. As an example it is demonstrated in [3] that by using measurement to control the transmissivity of a electro optic-modulator, the timescale over which a pre-prepared coherent state survives can be greatly increased. Within the field of superconducting circuits recent advances using amplifiers with sufficiently low noise levels [4] have made it possible to realize feedback within mesoscopic circuits. This makes it possible to realize feedback control of single suberconducting qubits. Demonstration of the feasibility of measurement-based feedback control in these systems were first shown by [5] and [6]. The range of mesoscopic systems used to study quantum control is constantly increasing and further interest have been shown to study control within other systems such silicon based on-chip optical devices as well as quantum dots [2].

Clearly the field of quantum control and quantum measurement is at this point in time a vast field of study, with an equally vast number of applications in most sub-fields of physics [2]. In recent years rapid experimental progress have been made in the ability to implement quantum measurement and control of mesoscopic systems. This progress have no sign of stopping and it is expected that only within a few years to see further advances in both the sophistication and accuracy of the feedback control protocols realized in laboratories around the world. However, the ability to efficiently control quantum systems have many further technological applications outside the main field of quantum information. For instance, in quantum thermodynamics, efficient control of quantum systems is crucial for performing information to energy conversion.

Within quantum control and control theory in general, one introduces the concept of a controller. This controller is constantly trying to achieve some predetermined objective. This objective can for example be to steer the system into a certain state or to optimize a transport process. Given an objective, the goal is then to find a rule for the controller to be able to achieve its goal, this rule is referred to as the feedback protocol. One of the most important properties of feedback is its ability to reduce noise in the system. By performing measurements we necessarily reduce our uncertainty of the system dynamics, but since there is no such thing as a free lunch this uncertainty or

randomness is necessarily transferred from the system to the memory of the measuring device of the controller. This implies something quite fundamental, since the amount of randomness of a system is related to entropy, feedback necessitates a way to reduce entropy of a system by transferring it to another system [2]. Hence, these kinds of feedback system are natural candidates for studying Maxwell demons.

The theory of quantum control have been in development since the the 80's. A large number of authors have independently derived equations for quantum control by continuous measurement based on stochastic differential equations [7][8]. These stochastic equations are generally not analytically solvable with solutions only numerically obtainable. A noticeable exception is the Wiseman-Milburn equation, derived by H. M. Wiseman and G. J. Milburn [9]. This equation is a Markovian master equation, i.e. the dynamics only depend on the current state of the system and possible memory effects are disregarded. The equation is able to treat feedback protocols were the protocol depends linearly on the measured signal. However, more often then not optimal control requires us to use non-linear protocols [10].

Björn Annby-Andersson et al. recently published a paper in which a novel formalism being able to describe the dynamics of a continuously feedback controlled quantum system is presented. The formalism describes a system connected to a measurement device where the measured signal is used in feedback to control the quantum system [11]. The formalism described the joint dynamics of system and detector and it can, in contrast to previous formalism, analytically treat non-linear feedback protocols, i.e feedback protocols that depend non-linearly on the measured signal used to implement the feedback protocol. This thesis has applied this formalism to new systems to investigate the formalism. The investigation was made through the analysis of two separate models, one classical model and one quantum model consisting of a double dot system using proposed feedback schemes. The transport properties of these two systems and the effect of the choice of feedback protocols on these properties was investigated using full counting statistics. This was done using analytical results obtained from a separation of timescales approximation approach as well as an exact numerical solution. The overall goal of the thesis was to demonstrate the property of feedback protocols to trade entropy between the system and the controller, hence demonstrating that it is possible to implement Maxwell demons using feedback. Furthermore, the aim is to find parameter regions where these systems acted as Maxwell demons and provide a proof of concept that information to energy conversion could be achived using the proposed feedback schemes.

This thesis is separated into 4 main parts. Chapter 2 is dedicated to introducing the relevant theory, deriving the Quantum Fokker-Planck master equation that underpins the work done in this thesis as well the other theoretical tools needed. Chapter 3 deals with application of the formalism to the classical system consisting of a single quantum dot, the system is presented together with the feedback scheme considered. Finally the results are presented and discussed. Chapter 4 is dedicated to the quantum double dot system. The system is presented together with the proposed feedback scheme. The obtained results are then presented and discussed. Chapter 5 is dedicated to conclusions and outlook.

Chapter 2

Theory

2.1 Maxwell's Demon & Information Engines

In 1929 Leo Szilard published a momentously important paper [12] in which a creature that had been demonizing physics since the late 19th century [13] was (seemingly) finally slain and in its wake a concrete link between thermodynamics and modern information theory was established. In the paper, a simple feedback scheme was analyzed, in which information obtained from measurements could be used to convert heat from a single heat bath into work, seemingly violating the 2nd law of thermodynamics. It was argued in the paper that the negative entropy production of this process was compensated by the entropy production of the feedback controller such that the 2nd Law is saved. However, this point remained quite controversial and was not considered settled until Rolf Landuer formulated his now famous principle [14]. The Landuer principle states that there is a lower bound on the minimum amount of heat required to erase information. This principle came out of a realization by Landuer, namely that the argument Szilard presented regarding the entropy production of the observer would not hold for measurements that are thermodynamically reversible where the observer would not need to expend energy to perform the measurement as was assumed by Szilard. Instead it was realized that the observer must have a memory storage. Assuming an initially blank memory, the memory must be cleaned in order to return to the initial state, meaning that information must be erased. This must necessarily generate entropy and hence once again save the 2nd law. Landuaer argued in his paper that the minimum heat required to erase a bit of information is given by $k_b T \log 2$. The existence of this "Landuer limit" of a minimum heat generation while erasing a bit of information as well as the possibility to convert information into heat have lately been experimentally verified [15][16].

This thesis considers feedback of quantum systems through continuous measurement to investigate transport properties of two separate systems. The point of this investigation is to find parameter regions where information engines can be constructed. For continuous measurement and feedback it is not formally possible to use Landuaer's principle as an explanation for not violating the 2nd law. There would necessarily be some continuous entropy production at the detector that can be treated for some models [11]. This thesis however is necessarily focused on showing a proof of concept for these two systems as well as investigating the properties of the dynamics obtained from the novel formalism considered.

2.2 Density matrices & Master equations

While it is often sufficient for closed quantum systems to work with the standard notion of states and wavefunctions this turns out to not necessarily be enough when considering open quantum systems, i.e systems where one takes into account the interaction between the system and its environment. With this approach we are limited to describing pure states while open quantum systems in general require us to be able to treat mixed state (representing a lack of knowledge of the initial preparation of the system) as well as entangled states which cannot be resolved into a pure state [17]. Hence, one instead makes use of a slightly generalized formulation of quantum mechanics where the state of the system of interest is represented by a new object called the density matrix. This object was first introduced by the mathematician John von Neuman [18] [19].

The density matrix for an ensemble of pure states [20] is defined by

$$\rho = \sum_i p_i \left|\psi_i\right\rangle \left\langle\psi_i\right| . \tag{2.1}$$

Where p_i are the probabilities to be in state $|\psi_i\rangle$. Thus, we now represent the state of the system by an operator. This operator represents our knowledge about a system, and corresponds to a probability distribution over classical states. Some important properties of the density matrix then immediately follows, taking the trace of ρ gives us

$$\mathrm{Tr}\{\rho\} = \sum_{i,j} p_i \left\langle\psi_j|\psi_i\right\rangle \left\langle\psi_i|\psi_j\right\rangle = \sum_i p_i = 1. \tag{2.2}$$

Hence, the sum of the diagonal elements of the density matrix is always one. The following properties also follows:

$$\text{Hermitian: } \rho^\dagger = \rho, \tag{2.3}$$

$$\text{Positive: } \left\langle\psi\right| \rho \left|\psi\right\rangle \geq 0 \; \forall \left|\psi\right\rangle . \tag{2.4}$$

The diagonal elements of the density matrix are called populations and represents the probability to be in that particular state that is part of the ensemble of states. The off-diagonal terms are instead referred to as coherence's and do not have any classical interpretation.

For a pure state $|\psi\rangle$ the time evolution is given by the Schrödinger equation

$$i\partial_t \left|\psi\right\rangle = \hat{H} \left|\psi\right\rangle . \tag{2.5}$$

Where $\hat{H}$ is the Hamiltonian. Taking the time derivative of our density matrix we can then write

$$\dot{\rho} = \sum_i p_i \left[\left(\partial_t \left|\psi_i\right\rangle\right) \left\langle\psi_i\right| + \left|\psi_i\right\rangle \left(\partial_t \left\langle\psi_i\right|\right)\right] = \frac{1}{i} \sum_i p_i \left[\hat{H} \left|\psi_i\right\rangle\!\!\left\langle\psi_i\right| - \left|\psi_i\right\rangle\!\!\left\langle\psi_i\right| \hat{H}\right], \tag{2.6}$$

$$\implies \dot{\rho} = \frac{1}{i} \left[H, \rho\right] .$$

Equation 2.2 is referred to as the von Neumann equation. We see that for a closed system the time evolution of the density matrix is given by its commutator with the Hamiltonian (As is typical for operators [21]). From this we can define a superoperator, known as the Liouville superoperator $\mathcal{L}$.

$$\dot{\rho} = \frac{1}{i}[\hat{H}, \rho] = \mathcal{L}\rho. \tag{2.7}$$

This equation has a formal solution

$$\rho(t) = e^{\mathcal{L}t}\rho(0), \tag{2.8}$$

if $\mathcal{L}$ is time independent. Hence, $e^{\mathcal{L}t}$ is analogous to a time evolution operator for the density matrix. The time-evolution we have described above holds for closed quantum systems i.e when there is no environment that can

influence the dynamics of our system. We are however interested in treating interactions with our environment, i.e describe a situation where the system can exchange energy and matter with the surrounding environment. Hence, we need a way to describe this kind of dynamics.

Our new Hamiltonian of interest could then in principle be written down as follows [22]

$$\hat{H}_{tot} = \hat{H}_S \otimes \mathbf{1}_B + \mathbf{1}_S \otimes \hat{H}_B + \hat{H}_I, \tag{2.9}$$

where $\hat{H}_S$ is the Hamiltonian of our system, $\hat{H}_B$ is a Hamiltonian of the environment, for example a thermal bath, and $\hat{H}_I$ is the hamiltonian describing the interaction between the system and the bath. $\mathbf{1}_B$ and $\mathbf{1}_S$ are the unit operator in the bath space and system space respectivly, representing that in the basis of product states the two different Hamiltonian's acts on the appropriate space. By making additional assumptions about the interaction with the environment, most importantly that the coupling between the environment and the system is weak, it is possible to derive what is known as the Gorini–Kossakowski–Sudarshan–Lindblad equation, or GKSL equation for short. This is the most general form of a Markovian master equation describing the evolution of a density matrix ρ that makes sure to preserve the laws of quantum mechanics (the equation preserves the properties of a density matrix). For more details the reader is referred to [23]. According to the GKSL equation the dynamics of the system when taking into account influence of the environment is given by [23]

$$\dot{\rho} = \frac{1}{i\hbar}\left[\hat{H}_s, \rho\right] + \sum_i L_i \rho L_i^\dagger - \frac{1}{2}\left\{L_i L_i^\dagger, \rho\right\} = \mathcal{L}\rho. \tag{2.10}$$

Here L_i are trace-less operators referred to as jump operators. These operators describe the interaction between the system and its environment (in this thesis the environment in question will always be ideal fermionic baths at certain temperature T and chemical potential μ and the jump operators will be given by the operators describing particle transport between the system and the reservoir). There are many different ways to motivate and/or derive this equation, slightly different approach and interesting discussion of the history behind the equation can be found in [24]

2.3 Generalized Quantum Measurements (POVM'S)

In order to implement feedback on our system one must necessarily extract information from the system. For instance, in order to control the temperature of a room it is necessary to have information about the current state of the temperature of the room. Usually when one talks about measurements in quantum mechanics one is referring to projective measurements or Von Neumann measurements. These kinds of measurements extracts perfect information about a system in the sense that given a measurement result using a non-degenerate observable, the state of the system is uniquely determined. This is referred to as the collapse of the wavefunction. However, for quantum systems this is not necessarily preferable since this leads to suppression of coherent dynamics. For continuous projective measurement, i.e when the measurement is performed rapidly such that the output of the measurement can be considered an continuous signal, this suppression is then often observed by the measurement process forcing the system into a particular state, a phenomenon known as the Zeno effect [25].

In order to avoid this problem it is needed to construct measurement operators that does not extract perfect information about the system i.e a weaker form of projective measurements, these measurements operators are what is referred to as weak measurements [26][27]. A convenient way to introduce weak measurements operators is to first make a detour into a more generalized form of measurement operators, known as POVM's (Positive operator valued measures).

POVM's are defined as a set of n operators $\{\Omega_n\}$ obeying the completeness relation $\sum_n \Omega_n^\dagger \Omega_n = \mathbf{1}$. By the fundamental theorem of quantum measurements [28] these operators describe a possible measurement on a system with n different outcomes, where the state after the measurement, given that we observed result n, is given by

$$\rho_n' = \frac{\Omega_n \rho \Omega_n^\dagger}{\mathrm{Tr}\left\{\Omega_n \rho \Omega_n^\dagger\right\}}, \tag{2.11}$$

where the probability to obtain result n is identified as $p_n = \mathrm{Tr}\{\Omega_n \rho \Omega_n^\dagger\}$. Equation 2.11 is the most general form for describing a quantum measurement and describes any type of measurement, including projective measurements. It can be shown that given an extra auxiliary system it is always possible to realize any generalized measurement using projective measurements (von Neumann Measurements) [29].

We will consider measurement operators that can be written as [11]

$$\hat{K}(d) = \left(\frac{2\lambda\delta t}{\pi}\right)^{1/4} e^{-\lambda\delta t(d-\hat{A})^2}, \tag{2.12}$$

satisfying

$$\int dd\hat{K}(d)^\dagger \hat{K} d) = \mathbf{1}. \tag{2.13}$$

We then update our state by

$$\rho'(d) = \hat{K}(d)\rho\hat{K}(d)^\dagger, \tag{2.14}$$

such that $\mathrm{Tr}\{\rho'(d)\}$ can be interpreted as the probability to have obtained measurement result d. Here $\hat{A}$ is our observable of interest, d is the measurement result and λ is the measurement strength parameter. We note that the effect of this weak measurement compared to a projective measurement is to spread a state around the average value of the observable. This becomes especially clear if we consider an observable with a continuous spectrum. As λ becomes larger, the Gaussian spread becomes smaller and smaller and in the limit of infinitely strong measurement the operator collapses to a projective measurement, of $\hat{A}$.

The assumption to consider a Gaussian form of the measurement operator may seem restrictive. However, it is guaranteed by the central limit theorem that any temporally course grained weak measurement, given by any POVM, will have Gaussian form, meaning that the Gaussian form is in fact quite general [29].

2.4 Feedback signal

In the continuous limit, we will obtain a time-continious measurement signal $d(t)$. This signal is too noisy in order for it to be useful to perform any kind of feedback schemes in a meaningful way [11]. In order to extract useful information from the signal, the output from our measurement is therefore processed. We therefore introduce a processed detector output $D(t)$ as

$$D(t) = D(t_0)e^{-\gamma(t-t_0)} + \gamma\int_{t_0}^{t} e^{\gamma(s-t)}d(s)ds. \tag{2.15}$$

Here we add some delay into the signal where the response rate of the processing is parameterized by γ. Here $1/\gamma$ sets a timescale for a delay that could be interpreted as a delay introduced by the circuitry of the detector. This is somewhat similar to the filtering proposed in [30].

We also note that equation 2.15 is the solution to $\dot{D} = \gamma(d - D)$, which is a differential equation that can be interpreted as the Langevin equation for the Orstein-Uhlenbeck process as described in [31]. The Ornstein-Uhlenbeck process is a stochastic process that shows up in different areas of physics. The process was originally used to model the velocities of Brownian particles affected by friction but in this case models the dynamics of the detector reaching a steady-state result. For more details the reader is referred to [31] and [32].

Since $d(t)$ comes from a Gaussian measurement, we can think of it as a stochastic variable written as $d(t) = m + \gamma\xi(t)/\sqrt{4\lambda}$. Where $\xi(t)$ is a normal distribution with zero mean and variance δt and m is the mean of $d(t)$. In this case we can rewrite our differential equation as

$$\dot{D}(t) = \gamma\left(m - D(t)\right) + \frac{\gamma}{\sqrt{4\lambda}}\xi(t). \tag{2.16}$$

Instead of thinking in terms of D(t) and instead considering the entire distribution $P(D,t)$ it is possible to convert this Langevin equation into a Fokker-Planck equation. A Fokker-Planck equation is a partial differential equation that describes the time evolution of a probability density [31], which in this case is the probability density of the obtained measurement results. This Fokker-Planck equation will be important below.

2.5 Derivation of Formalism: Part I

We now perform a derivation of the feedback master equation that is at the center of this project, the derivation closely follows the work done in [11]. It is handy to define the following superoperator

$$\mathcal{M}(d)\rho = K(d)\rho K^{\dagger}(d), \tag{2.17}$$

where $K(d)$ represents the measurement operator for outcome d and $\mathcal{M}(d)\rho$ is the state of the system after measuring d. We need to take into account not the raw signal $d(t)$ but the processed signal $D(t)$. This is done by appropriate use of delta functions. Let t_0 be the starting time for the system and discretize time into chunks of δt such that a time t_k is the time after taking k timesteps after t_0, i.e $t_k = t_0 + k\delta t$. The (now discrete) processed signal $D(t_k)$ will depend on all the previous raw signals $d(t)$ at the timesteps since t_0. From the above discussion about the processing of the raw signal we see that the discrete processed signal after k timesteps since t_0 can be written as

$$D(t_k) = f(d_1, ..., d_k) = D(t_0)e^{-\gamma k\delta t} + \gamma\delta t\sum_{i=1}^{k} e^{\gamma(i-k)}d_i. \tag{2.18}$$

Now imagine the following process: we time evolve the system by δt and then perform a measurment with some outcome d_1. We then continue time evolving another timestep then measuring and so on and on and on... After n steps of this process has been done we can write the resulting density matrix as

$$\rho(t, d_1, ..., d_n) = \mathcal{M}(d_n)e^{\mathcal{L}\delta t}\ldots\ \mathcal{M}(d_1)e^{\mathcal{L}\delta t}\rho(t_0), \tag{2.19}$$

where we explicitly write out in the LHS that the resulting density matrix depends on the n measurement results d_n. Note that the state on the LHS is not normalized as described above. Taking the trace gives the probability to have obtained the detector results d_1 through d_n at the time t. However, as discussed above we are not interested in the raw signal output $d(t)$ but the processed signal. Since we are also interested in being able to incorporate feedback we need to allow the time-evolution operators to be able to depend on the processed signal $D(t)$.

To this end, we write

$$\rho(t, D_1, ..., D_n) = \int .. \int dd_1..dd_n\mathcal{M}(d_n)e^{\mathcal{L}(D_{n-1})\delta t}\ldots\ e^{\mathcal{L}(D_1)\delta t}\mathcal{M}(d_1)e^{\mathcal{L}\delta t}\rho(t_0)\delta(D_n - f(d_1, ..., d_n))...\delta(D_1 - f(d_1)), \tag{2.20}$$

where the delta functions makes sure that D_k is consistent with Eq. (2.18). We can perform the integration over the $d_k's$ with the help of the delta functions using the following identity

$$\delta(f(x)) = \sum_i \frac{\delta(x - x_i)}{|f'(x_i)|}, \tag{2.21}$$

where x_i are the solutions to $f(x) = 0$. The delta functions are of the form

$$\delta(D_k - f(d_1, ..., d_k)). \tag{2.22}$$

We can then define

$$g(d_k) = (D_k - f(d_1, ..., d_k)). \tag{2.23}$$

Giving

$$g(d_k) = 0 \implies D_k - [D(t_0)e^{-\gamma k\delta t} + \gamma\delta t\sum_{i=1}^{k-1} e^{\gamma(i-k)\delta t}d_i] - \gamma\delta t d_k = 0 \tag{2.24}$$

$$\implies D_k - e^{-\gamma\delta t}\underbrace{[D(t_0 e^{-\gamma(k-1)\delta t} + \gamma\delta t\sum_{i=1}^{k-1} e^{\gamma(i-k-1)\delta t} d_i]}_{D_{k-1}} - \gamma\delta t d_k = 0.$$

So finally we get

$$d_k = \frac{D_k - D_{k-1}e^{-\gamma\delta t}}{\gamma\delta t} \quad \text{and} \quad g'(d_k) = -\gamma\delta t. \tag{2.25}$$

Carrying out the integrals in (2.20) yields

$$\rho(t, D_1, ..., D_n) = \frac{1}{(\gamma\delta t)^n}\mathcal{M}\left(\frac{D_n - D_{n-1}e^{-\gamma\delta t}}{\gamma\delta t}\right) e^{\mathcal{L}(D_{n-1})\delta t} \dots\ e^{\mathcal{L}(D_1)\delta t}\mathcal{M}\left(\frac{D_1 - D_0 e^{-\gamma\delta t}}{\gamma\delta t}\right) e^{\mathcal{L}\delta t}\rho(t_0). \tag{2.26}$$

Here it is convenient to define

$$\mathcal{M}(D|D') = \mathcal{M}\left(\frac{D - D'e^{-\gamma\delta t}}{\gamma\delta t}\right)\frac{1}{\gamma\delta t}. \tag{2.27}$$

In the end we are only interested in $\rho(t, D_n)$ i.e the system at time t given a processed signal D_n. To do this we integrate out the previous steps

$$\rho(t, D_n) = \int ... \int dD_1 ... dD_{n-1}\rho(t, D_1, ..., D_n) \tag{2.28}$$

$$= \int dD_{n-1}\mathcal{M}(D_n|D_{n-1})e^{\mathcal{L}(D_{n-1})\delta t} \times$$

$$\int .. \int dD_{n-2}dD_1 \underbrace{\mathcal{M}\left(D_{n-1}|D_{n-2}\right) e^{\mathcal{L}(D_{n-2})\delta t} ... e^{\mathcal{L}(D_1)\delta t}\mathcal{M}\left(D_1|D_0\right)) e^{\mathcal{L}\delta t}\rho(t_0)}_{\rho(t-\delta t, D_1, .., D_n)}$$

$$= \int dD_{n-1}\mathcal{M}(D_n|D_{n-1})e^{\mathcal{L}(D_{n-1})\delta t}\rho(t - \delta t, D_{n-1}). \tag{2.29}$$

Hence, we finally end up with

$$\boxed{\rho(t + \delta t, D) = \int dD'\mathcal{M}(D|D')e^{\mathcal{L}(D')\delta t}\rho(t, D').} \tag{2.30}$$

Where the identifications $D = D_n$, $D_{n-1} = D'$, $t = t + \delta t$ have been made.

2.6 Derivation of Formalism: Part II

In order to make analytical calculations more manageable it is favourable to expand the measurement operator $\mathcal{M}(D|D')$ in equation 2.30 to first order in δt. We therefore examine how this measurement operator acts on a state ρ

$$\mathcal{M}(D|D')\rho = \left(\frac{2\lambda}{\pi\gamma^2\delta t}\right)^{1/2} \iint dada' e^{-\lambda\delta t\left(\frac{D - D'e^{-\gamma\delta t}}{\gamma\delta t} - \hat{A}\right)}\rho_{a,a'}\left|a\right\rangle\left\langle a'\right| e^{-\lambda\delta t\left(\frac{D - D'e^{-\gamma\delta t}}{\gamma\delta t} - \hat{A}\right)}, \tag{2.31}$$

where we have inserted the definition of the Gaussian measurement operators and expanded ρ in the eigenbasis of the observable $\hat{A}$. Continuing we get

$$\mathcal{M}(D|D')\rho = \left(\frac{2\lambda}{\pi\gamma^2\delta t}\right)^{1/2} \iint dada' e^{-\lambda\delta t\left(\frac{D - D'e^{-\gamma\delta t}}{\gamma\delta t} - a\right)} e^{-\lambda\delta t\left(\frac{D - D'e^{-\gamma\delta t}}{\gamma\delta t} - a'\right)}\rho_{a,a'}\left|a\right\rangle\left\langle a'\right|. \tag{2.32}$$

After some algebra the exponents of the two exponentials simplifies to

$$\mathcal{M}(D|D')\rho = \left(\frac{2\lambda}{\pi\gamma^2\delta t}\right)^{1/2} \iint dada' e^{-\frac{1}{2}\lambda\delta t(a-a')^2} e^{-2\lambda\delta t\left(\frac{D-D'e^{-\gamma\delta t}}{\gamma\delta t} - \frac{a+a'}{2}\right)^2} \rho_{a,a'} \left|a\right\rangle\!\left\langle a'\right|. \tag{2.33}$$

Here we can make use of an interesting trick, namely that the second exponential in equation 2.33 can be written as an inverse Fourier transform. First we must make use of for small δt we have $e^{-\gamma\delta t} \approx 1 - \gamma\delta t$ which then gives us

$$\sqrt{\frac{2\lambda}{\pi\gamma^2\delta t}} e^{-\frac{1}{2}\lambda\delta t(a-a')^2} e^{-\frac{2\lambda}{\gamma^2\delta t}\left(D-D' - \frac{\gamma\delta t(a+a')}{2} - \gamma\delta t D'\right)^2} = \tag{2.34}$$

$$\frac{1}{2\pi}\int_{-\infty}^{\infty} d\omega e^{-\frac{1}{2}\lambda\delta t(a-a')^2} e^{\frac{\omega\delta t}{8}\left(4i\gamma(a+a') - \frac{\gamma^2\omega}{\lambda} - 8i\gamma D'\right)} e^{-i\omega(D-D')}.$$

To first order in δt the integrand then becomes

$$\approx \left[1 - \frac{1}{2}\lambda\delta t(a-a')^2 + \frac{1}{8}\omega\delta t\left(4i\gamma(a+a') - \frac{\gamma^2}{\lambda}\omega - 8i\gamma D'\right)\right] e^{-i\omega(D-D')}. \tag{2.35}$$

We can the perform the integral over ω identifying the following identities for the inverse fourier transform

$$\delta(x) = \frac{1}{2\pi}\int d\omega e^{-i\omega x} \quad \delta'(x) = -\frac{i}{2\pi}\int d\omega\omega e^{-i\omega x} \quad \delta''(x) = -\frac{1}{2\pi}\int d\omega\omega^2 e^{-i\omega x}. \tag{2.36}$$

Giving us the RHS of (2.31)

$$\iint dada'\left[\left(1 - \frac{\lambda\delta t}{2}(a-a')^2\right)\delta(D-D') - \left(\frac{\gamma\delta t}{2}D' + \frac{\lambda\delta t}{2}(a-a')^2\right)\delta'(D-D') - \frac{\gamma^2\delta t}{8\lambda}\delta''(D-D')\right]\rho_{a,a'}\left|a\right\rangle\!\left\langle a'\right|. \tag{2.37}$$

Using identities derived in appendix 6.1 we can then perform the integration over a, a' and rewrite the equation on operator form as

$$\delta(D-D')\rho + \lambda\delta t\delta(D-D')\left(\hat{A}\rho\hat{A} - \frac{1}{2}\left\{\hat{A}\hat{A},\rho\right\}\right) + \gamma\delta t D'\delta'(D-D')\rho - \frac{1}{2}\gamma\delta t\delta'(D-D')\left\{\hat{A},\rho\right\} + \frac{\gamma^2}{8\lambda}\delta t\delta''(D-D')\rho. \tag{2.38}$$

Plugging this back into equation 2.30 and taking the limit $\delta t \to 0$ we then finally get our master equation

$$\boxed{\partial_t\rho(t,D) = \mathcal{L}(D)\rho(t,D) + \lambda\mathcal{D}[\hat{A}]\rho(t,D) - \gamma\partial_D\mathcal{A}(D)\rho(t,D) + \frac{\gamma^2}{8\lambda}\partial_D^2\rho(t,D)} \tag{2.39}$$

Where $\mathcal{D}[\hat{A}] = \hat{A}\rho\hat{A} - \frac{1}{2}\left\{\hat{A}\hat{A},\rho\right\}$ and $\mathcal{A}(D)\rho = \frac{1}{2}\left\{\hat{A} - D,\rho\right\}$.

We quickly comment on the obtained equation since the different terms have quite clear interpretations. The first term on the RHS is simply the Liouvillian for the system but now dependent on the processed measurement signal $D(t)$, hence making feedback implementations possible. The second term is the back-action term from the continuous measurement. Note that the effect of the measurement enters as a dissipator. Thus, the effect of the measurement enters in the same way as environmental interactions does in the GKSL equation. The last two terms is the Fokker-Planck equation for the Ornstein-Uhlenbeck process describing our processed measurement signal.

2.7 Separation of Timescales

In order to make analytical calculations possible several approximation will be made. The main idea of these approximation is to assume that the timescale of the detector and the timescale of the system evolution are very

different. Looking back at equation (2.39) we can identify the following timescales

$$\partial_t \rho(t,D) = \underbrace{\mathcal{L}\rho(t,D)}_{\frac{1}{\tau_s}} + \underbrace{\lambda\mathcal{D}[\hat{A}]\rho(t,D)}_{\tau_{b.a}=\lambda^{-1}} - \underbrace{\gamma\partial_D\mathcal{A}\rho(t,D)}_{\tau_{\text{detector}}=\gamma^{-1}} + \frac{\gamma^2}{8\lambda}\partial_D^2\rho(t,D). \tag{2.40}$$

Where τ_s is the timescale of the Liouvillian, similarly for $\tau_{\text{b.a}}$ and τ_{detector}. The crucial approximation is to assume that the detector timescale $\frac{1}{\gamma}$ is much smaller then the time scale for the time evoultion of the system τ_s as well as the timescale for the dephasing from the back-action $\frac{1}{\lambda}$. In the limit $\gamma \gg \lambda, \tau_s^{-1}$ our equation simplifies to

$$\partial_t \rho(t,D) \approx -\gamma\partial_D\mathcal{A}\rho(t,D) + \frac{\gamma^2}{8\lambda}\partial_D^2\rho(t,D). \tag{2.41}$$

We continue by writing ρ in the eigenbasis of the measurement operator

$$\sum_{a,a'} \dot{\rho}_{a,a'}(t,D)\,|a\rangle\langle a'| = \sum_{a,a'}\left[-\gamma\frac{\partial}{\partial D}\left(\frac{a+a'}{2} - D\right)\rho_{a,a'}(D,t) + \frac{\gamma^2}{8\lambda}\frac{\partial^2}{\partial D^2}\rho_{a,a'}(t,D)\right]|a\rangle\langle a'|\,. \tag{2.42}$$

We note that in this limit the components $\rho_{a,a'}(t,D)$ are solutions to the Fokker-Planck equation for the Ornstein-Uhlenbeck process [33]. A detailed solution to this equation is found in [31]. Assuming the initial condition $\rho_{a,a'}(t_0,D) = \rho_{a,a'}(t_0)\delta(D-D_0)$ the full solution can be written as

$$\rho_{a,a'}(t,D) = \sqrt{\frac{4\lambda\rho_{a,a'}^2(t_0)}{\pi\gamma\left(1-e^{-2\gamma(t-t_0)}\right)}}exp\left(\frac{4\lambda}{\pi\gamma\left(1-e^{-2\gamma(t-t_0)}\right)}\left[D - \frac{a+a'}{2}(1-e^{-\gamma(t-t_0)} - D_0e^{-\gamma(t-t_0)}\right]^2\right). \tag{2.43}$$

The second approximation we can make at this point is to assume that the detectors is sufficently fast such that all transients of the measurement process have died out and that the detector is constantly in steady state, the steady state solution is obtained by

$$\rho_{a,a'}(D) = \lim_{t\to\infty}\rho_{a,a'}(t,D) = \sqrt{\frac{4\lambda}{\pi\gamma}}e^{-\frac{4\lambda}{\gamma}\left(D-\frac{a+a'}{2}\right)^2}\rho_{a,a'}(t_0). \tag{2.44}$$

In the above equation we note that the detector behaviour given the assumptions stated above can effectively be decoupled from the time dependent part of equation (2.39). The idea is now to use this to try and find separable solutions to the problem i.e we try to find solutions of the form

$$\rho(t,D) = \rho(t)G(D) = \sum_{a,a'} G_{a,a'}(D)\rho_{a,a'}\,|a\rangle\langle a'|\,. \tag{2.45}$$

Where we in the last line have expanded the solution in the eigenbasis of the measurement operator $\hat{A}$ and introduced the detector function $G(D)$ describing a probability density of getting the measurement outcome D. Plugging this ansatz back into equation 2.39 we get

$$\sum_{a,a'} G_{a,a'}(D)\dot{\rho}_{a,a'}\,|a\rangle\langle a'| = \sum_{a,a'} G(D)_{a,a'}\rho_{a,a'}(t)\left[\mathcal{L}(D)\,|a\rangle\langle a'| + \lambda\mathcal{D}[\hat{A}]\,|a\rangle\langle a'|\right]. \tag{2.46}$$

We can then integrate the LHS and RHS over D to get (since $G_{a,a'}$ is normalized)

$$\frac{\partial}{\partial t}\rho(t) = \lambda\mathcal{D}[\hat{A}]\rho(t) + \int dD'\mathcal{L}(D')\left(\sum_{a,a'} G_{a,a'}\mathcal{P}_{a,a'}\right)\rho(t). \tag{2.47}$$

Where the density matrix once again is written without respect to a basis and the projector $\mathcal{P}_{a,a'}$ has been introduced, which has the property $\mathcal{P}_{a,a'}\rho = \rho_{a,a'}|a\rangle\langle a'|$. We can introduce a new superoperator $\tilde{\mathcal{L}}$ such that we can formally write down a solution to 2.47 as

$$\rho(t) = e^{\tilde{\mathcal{L}}t}\rho(0) \quad \text{with} \quad \tilde{\mathcal{L}} = \lambda\mathcal{D}[\hat{A}] + \int dD'\mathcal{L}(D')\left(\sum_{a,a'} G_{a,a'}\mathcal{P}_{a,a'}\right). \tag{2.48}$$

So under the seperation of timescale approximation the result is a decoupling of the system and detector dynamics where the time evolution of the system is given by a new superoperator which consists of averaging over the old Liouvillan and an additional dissipator term.

We stop to make a short remark on the classical limit of this equation. In this limit when only the diagonal elements of the density matrix are considered one can find analytical solutions to 2.47 for some feedback schemes. Note that the dissipator term in the equation vanishes in the classical limit when working in the eigenbasis of the measurement operator, this is seen by

$$\lambda\mathcal{D}[\hat{A}]\rho = \lambda\left(\hat{A}\rho\hat{A} - \frac{1}{2}\{\hat{A}^2,\rho\}\right) = \sum_{a,a'}\underbrace{\delta_{a,a'}\rho_{a,a'}|a\rangle\langle a'|}_{\text{Classical limit}}\left[aa' - \frac{1}{2}\left(a^2 + a'^2\right)\right] = 0. \tag{2.49}$$

However, we should not be surprised that a quantum mechanical effect (the back-action from the measurement) vanishes when considering a classical limit.

2.8 Full Counting Statistics

In order to further investigate the systems we will be considering, we will be needing methods to obtain information of the statistics of the processes involved. Usually we are interested in the statistics of the electron transport in these systems. That is, we want to know how many electrons n, on average, that have traversed the system after some time t. Typically, we are interested in knowing the full distribution $P^{(n)}(t)$ of n. To find this distribution, we will employ the method of full counting statistics (FCS). The following derivations closely follows what is done in [34].

Consider the on-diagonal terms of our typical master equation which as we have seen are interpreted as classical probabilities

$$\dot{\rho}_{ii} = \sum_j \mathcal{L}_{ij}\rho_{jj} \implies \dot{P}_i = \sum_j \mathcal{L}_{ij}P_j. \tag{2.50}$$

The matrix element $\mathcal{L}_{ij}$ represents the rate of the process of going from state j into state i, and associate to each such state a particle number n_i. A term like $\mathcal{L}_{ij}$ represents the a transport of $|n_i - n_j|$ particles to or from a reservoir. In the weak coupling limit, where our Lindblad formalism is valid [34], the transport is limited such that $|n_i - n_j| \in \{0, \pm 1\}$. We further form the joint probability $P_i^{(n)}$ of being in state i and having n traversed electrons. The idea is now to separate equation 2.50 into the three possible processes, those that leave n unchanged and those that either increase or decrease n by 1. With this in mind we can write down our new rate equation

$$\dot{P}_i^{(n)} = \sum_{j,\omega\neq\Omega}\mathcal{L}_{ij}^{\omega}P_j^{(n)} + \mathcal{L}_{ii}^{\Omega}P_{ii}^{(n)} + \sum_{j\neq i}\mathcal{L}_{ij}^{\Omega}P_j^{(n-n_j+n_i)}. \tag{2.51}$$

The first term of the RHS represent transitions to reservoir $\omega \neq \Omega$ that does not change n, the second term describes transitions to the same state. Finally $\mathcal{L}_{ij}^{\Omega}$ describes transitions that increase or decrease n. If we start in n_j and go to n_i that means that the change in reservoir number must be $|n_i - n_j|$. In order to end up with n traversed particles we must have started in $n + n_i - n_j$. We can now write this as a vector equation introducing the vector

$$\rho^{(n)} = \left(P_1^{(n)}, ..., P_d^{(n)}\right)^T. \tag{2.52}$$

Note that $\rho^{(n)}$ is just a vector of the classical probabilities of the density matrix conditioned on the number of traversed particles. We also separate $\mathcal{L}$ into the parts that change n as well as keep it constant

$$\dot{\rho}^{(n)} = \mathcal{L}_0\rho^{(n)} + \mathcal{L}_+\rho^{(n-1)} + \mathcal{L}_-\rho^{(n+1)}. \tag{2.53}$$

Here one makes use of a trick: we introduce the Discrete Fourier Transform

$$\rho(\chi, t) = \sum_n \rho^{(n)}(t)e^{in\chi}, \tag{2.54}$$

where we introduced the parameter χ, knows as a counting field. The inverse transform is

$$\rho^{(n)} = \frac{1}{2\pi}\int_{-\pi}^{\pi} \rho(\chi, t)e^{-in\chi}d\chi. \tag{2.55}$$

Transforming equation 2.53 gives

$$\dot{\rho}(\chi) = \underbrace{\left[\mathcal{L}_0 + \mathcal{L}_+e^{i\chi} + \mathcal{L}_-e^{-i\chi}\right]}_{\mathcal{L}_\chi}\rho(\chi). \tag{2.56}$$

This master equation has the solution

$$\rho(t, \chi) = e^{\mathcal{L}_\chi t}\rho(\chi, 0) \quad \text{with} \quad \rho^{(n)}(0) = \rho_0(0)\delta_{n,0} \text{ (No transport has occurred at } t = 0). \tag{2.57}$$

Then we get the full distribution

$$P^{(n)}(t) = \sum_i P_i^{(n)} = \mathrm{Tr}\Big\{\rho^{(n)}(t)\Big\} = \frac{1}{2\pi}\int_{-\pi}^{\pi} \mathrm{Tr}\big\{e^{\mathcal{L}_\chi t}\rho(\chi, 0)\big\}e^{-in\chi}. \tag{2.58}$$

If we want to find the moments for n we can therefore write

$$\begin{aligned}\langle n^k\rangle = \sum_{n,i} n^k P_i^{(n)} &= \left(-i\frac{\partial}{\partial\chi}\right)^k \mathrm{Tr}\left\{\sum_n \rho^{(n)}e^{i\chi n}\right\}\Big|_{\chi=0} = \left(-i\frac{\partial}{\partial\chi}\right)^k \mathrm{Tr}\{\rho(t, \chi)\}\Big|_{\chi=0} \\ &= \left(-i\frac{\partial}{\partial\chi}\right)^k \mathrm{Tr}\big\{e^{\mathcal{L}_\chi t}\rho(\chi, 0)\big\}\Big|_{\chi=0}.\end{aligned} \tag{2.59}$$

We then define the Moment generating function (MGF)

$$\boxed{\langle n^k\rangle = \left(-i\frac{\partial}{\partial\chi}\right)^k \mathcal{M}(\chi, t)\Big|_{\chi=0} \text{ with } \mathcal{M}(\chi, t) = \mathrm{Tr}\big\{e^{\mathcal{L}_\chi t}\rho(\chi, 0)\big\}} \tag{2.60}$$

Often we will be interested in the cumulants, therefore it is also convenient to define a Cumulant generating function

$$\boxed{\mathcal{C}(\chi, t) = \ln \mathcal{M}(\chi, t).} \tag{2.61}$$

Consider as an example the second cumulant i.e the variance of n. Using the CGF we get

$$(-i)^2\frac{\partial^2}{\partial\chi^2}\mathcal{C}\Big|_{\chi=0} = -\frac{\partial^2}{\partial\chi^2}\ln \mathcal{M}(\chi, t)\Big|_{\chi=0} = -\left\{\frac{\mathcal{M}''(\chi)}{\mathcal{M}(\chi)} - \frac{(\mathcal{M}'(\chi))^2}{\mathcal{M}^2(\chi)}\right\}\Big|_{\chi=0} = \langle n^2\rangle - \langle n\rangle^2 = \mathrm{Var}(n). \tag{2.62}$$

(Note that $\mathcal{M} = 1$ by trace preservation) the same relation holds for higher cumulants [34]. However, we are not only interested in the statistics of n but are more concerned with the current of the system i.e $\dot{n}$. For the current we find the first moment by

$$\langle\dot{n}(t)\rangle = -i\partial_\chi\frac{d}{dt}\mathrm{Tr}\Big\{e^{\mathcal{L}(\chi)t}\rho_0\Big\}\Big|_{\chi=0} = -i\partial_\chi\,\mathrm{Tr}\Big\{\mathcal{L}(\chi)e^{\mathcal{L}(\chi)t}\rho_0\Big\}\Big|_{\chi=0} \tag{2.63}$$

$$= -i\,\mathrm{Tr}\Big\{\mathcal{L}'(\chi)e^{\mathcal{L}(\chi)t}\rho_0 + \mathcal{L}(\chi)\partial_\chi e^{\mathcal{L}(\chi)t}\rho_0\Big\}\Big|_{\chi=0} = -i\,\mathrm{Tr}\Big\{\mathcal{L}'(\chi)e^{\mathcal{L}(\chi)t}\rho_0\Big\}\Big|_{\chi=0}.$$

Where the last term after the third equal sign vanishes due to the trace preserving nature of $\mathcal{L}$, that is $\mathrm{Tr}\{\mathcal{L}\sigma\} = 0$ for any vector σ. Finding the variance of the current can then be made in an analogous way.

Often we are not interested in the time evolution of the different cumulants but mainly interested in their steady state. Consider the Jordan form of $\mathcal{L}(\chi)$ given by

$$J = S\mathcal{L}(\chi)S^{-1}. \tag{2.64}$$

The key assumption to make at this point is to assume that the system governed by $\mathcal{L}$ only have one steady-state solution (which is valid for most systems). This means that the corresponding eigenvalue of the steady state eigenvector ρ_{ss} must be zero since by definition

$$\dot{\rho}_{ss} = \mathcal{L}\rho_{ss} = \lambda\rho_{ss} = 0. \tag{2.65}$$

However, note that $\mathcal{L}(\chi)$ does not necessarily have the same eigenvalues as $\mathcal{L}$, but we know that they must coincide as $\chi \to 0$. Because of this we can identify the eigenvalue of the steady state solution as the eigenvalue of $\mathcal{L}(\chi)$ that vanishes as χ is set to zero. We can now write our MGF as

$$\mathcal{M} = \mathrm{Tr}\Big\{e^{\mathcal{L}(\chi)t}\rho_0\Big\} = \mathrm{Tr}\big\{S^{-1}e^{Jt}S\rho_0\big\} = e^{\lambda(\chi)t}\,\mathrm{Tr}\Big\{S^{-1}e^{\tilde{J}}S\rho_0\Big\} = e^{\lambda(\chi)t}R(\chi), \tag{2.66}$$

where we in the second to last equality have factored out the eigenvalue of interest and then bundled up the rest of the expression in a new function $R(\chi)$. We then find that the CGS is given by

$$\mathcal{C} = \ln\mathcal{M} = \lambda(\chi)t + \ln R(\chi). \tag{2.67}$$

Since $\lambda(\chi)$ was supposed to be the only eigenvalue that vanishes as χ goes to zero and is supposed to be the eigenvalue corresponding to the steady state solution, all other eigenvalues must have non-vanishing negative real part even as χ goes to zero. Thus, in the large time limit e^{Jt} must have only one non-zero element on the diagonal corresponding to our eigenvalue of interest, while the rest is zero [34]. Motivating us to write in the large time limit (since what remains in $\ln R(\chi)$ will become negligible in this limit)

$$\mathcal{C} \approx \lambda(\chi)t. \tag{2.68}$$

At this point it then becomes trivial to find the cumulants of the current distribution

$$\left[\left(-i\frac{\partial}{\partial\chi}\right)^k \frac{\partial}{\partial t}\mathcal{C}\right]\Big|_{\chi=0} = (-i)^k\lambda^{(k)}(0). \tag{2.69}$$

2.8.1 Cumulant expansion

Sometimes even finding $\mathcal{C}$ for a complicated form of $\mathcal{L}$ may be more or less impossible. However, there is another trick we can make use off. Finding the characteristic polynomial of $\mathcal{L}$ is straight forward, this can be used to find the cumulants order by order. Let's consider the characteristic polynomial up to order 2

$$\mathcal{O}\big(\lambda^3\big) + C_2(\chi)\lambda^2(\chi) + C_1(\chi)\lambda(\chi) + C_0(\chi) = 0. \tag{2.70}$$

The eigenvalues of $\mathcal{L}$ are the solutions to this equation, but we are interested in the eigenvalue that vanishes as $\chi \to 0$. Let's take the first derivative of this equation w.r.t χ,

$$\mathcal{O}\big(\lambda^2\big) + C_2'\lambda^2 + 2C_2\lambda\lambda' + C_1'\lambda + C_1\lambda' + C_0' = 0. \tag{2.71}$$

Now take χ to zero and we end up with

$$C_1\lambda' + C_0' = 0 \implies \lambda' = -\frac{C_0'(0)}{C_1(0)}. \tag{2.72}$$

Using relation 2.69 we see that we get the first moment of the current. This can naturally be done to arbitrary order, this project will consider an expansion up to order 2, which is found to be given by

$$\lambda'' = -\frac{C_0'' + 2C_2\lambda'^2 + 2C_1'\lambda'}{C_1} = -\frac{C_0''(0)}{C_1(0)} - 2\frac{C_2(0)C_0'(0)^2}{C_1(0)^3} + 2\frac{C_1'(0)C_0'(0)}{C_1(0)^2}. \tag{2.73}$$

2.9 Numerical Approach

In order to be able to compare the analytical results obtained through the separation of timescales approximation, we employ a numerical scheme in order to fully solve equation 2.39. The method employed in this thesis is the general method outlined in [11]. The method consists of expanding the D-dependent density matrix in the following series of polynomials

$$\rho(D) = \sum_n M_n \frac{H_{e_n}^{[\sigma]}(D)}{\sqrt{\sigma^n n!}} \frac{e^{-D^2/2\sigma}}{\sqrt{2\pi\sigma}}, \tag{2.74}$$

where $H_{e_n}^{[\sigma]}(D)$ are rescaled probabalist Hermite polynomials, defined in terms of the standard physicist's Hermite polynomials $H_n(D)$ by

$$H_{e_n}^{[\sigma]}(D) = \left(\frac{\sigma}{2}\right)^{n/2} H_n\left(\frac{D}{\sqrt{2\sigma}}\right) \tag{2.75}$$

and M_n is the matrix corresponding to the form of ρ for that particular problem. For a full quantum 2 level problem M_n is given by

$$M_n = \begin{pmatrix} a_n & c_n \\ c_n^* & b_n \end{pmatrix}. \tag{2.76}$$

Here σ is chosen as $\gamma/8\lambda$ such that the Gaussian component of the ansatz matches the form for the solution to the Ornstein-Uhlenbeck process.

The polynomials fulfill the orthogonality condition [35]

$$\int dD \frac{H_{e_n}^{[\sigma]}(D)}{\sqrt{\sigma^n n!}} \frac{H_{e_m}^{[\sigma]}(D)}{\sqrt{\sigma^m m!}} \frac{e^{-D^2/2\sigma}}{\sqrt{2\pi\sigma}} = \delta_{n,m}. \tag{2.77}$$

This particular choice of polynomials is also very convenient since $H_{e_0}^{[\sigma]} = 1$ we get by the orthogonality condition

$$\rho = \int dD\rho(D) = \int dD \sum_n M_n \frac{H_{e_n}^{[\sigma]}(D)}{\sqrt{\sigma^n n!}} \frac{e^{-D^2/2\sigma}}{\sqrt{2\pi\sigma}} = M_0. \tag{2.78}$$

The normalization condition $\mathrm{Tr}\{\rho\} = 1$ is then reduced to $\mathrm{Tr}\{M_0\} = 1$.

Since we are only interested in the steady state solution for the systems considered in this thesis, the general numerical scheme consists of plugging in our ansatz 2.74 into equation 2.39. By multiplying the RHS by $H_{e_n}^{[\sigma]}$ and integrating over D (Up to the maximum n considered in the expansion). This process will in turn generate a homogeneous system of equations in terms of the components of ρ in the expansion, which can then readily be solved using standard methods part of most numerical packages (This thesis used the null space function part of the sci.py linalg package [36]).

When constructing the homogeneous equation system the following integral relation proved useful (which can be derived from the properties of the Hermite polynomials [35])

$$I_{mn} = \int_0^\infty dD \frac{H_{e_n}^{[\sigma]}(D)}{\sqrt{\sigma^n n!}} \frac{H_{e_m}^{[\sigma]}(D)}{\sqrt{\sigma^m m!}} \frac{e^{-D^2/2\sigma}}{\sqrt{2\pi\sigma}}. \tag{2.79}$$

With

$$I_{mn} = \begin{cases} 1/2 \text{ if } n = m \\ C_{nm}, \text{ if } n + m \text{ odd} \\ 0 \text{ else} \end{cases} \quad \text{and } C_{nm} = \frac{(-1)^{(n+m-1)/2} m!!\,(n-1)!!}{\sqrt{2\pi n!\, m!}(m-n)} \text{ (For even } n \text{ and odd } m). \tag{2.80}$$

Chapter 3

Classical system - Single Electron Transistor (S.E.T.)

3.1 Model & Feedback scheme

In this chapter, we consider a simple system consisting of a single level quantum dot coupled to two fermionic reservoirs at temperatures T_L and T_R and chemical potentials μ_L and μ_R, respectivly. The quantum dot is coupled to the reservoirs with tunneling rates Γ_L and Γ_R respectivly.

We will investigate if measurement of the occupation of the dot can be used in order to perform feedback control of the different transition rates in order to create an electronic pump and if we can operate this pump against the natural direction of the current, i.e if the temperatures of the two islands are kept the same can we move electrons against a chemical potential gradient when $T_L = T_R$.

We introduce the parameter

$$\Delta\mu = \mu_R - \mu_L. \tag{3.1}$$

We will consider this chemical bias as being applied symmetrically for the two reservoirs in such a way that we can write $\mu_L = -\Delta\mu/2$ and $\mu_R = \Delta\mu/2$, the Fermi functions evaluated at the energy of the dot are then given by

$$f_L = \frac{1}{e^{\Delta\mu/2k_BT}+1}, \quad f_R = \frac{1}{e^{-\Delta\mu/2k_BT}+1}. \tag{3.2}$$

The measurement operator in this case is given by the pauli-z operator σ_z and we will work in the eigenbasis $|0\rangle, |1\rangle$ of σ_z where $|0\rangle$ and $|1\rangle$ correspond to a vaccant and occupied quantum dot respectivly. A schematic description of the model is given in figure 3.1 below.

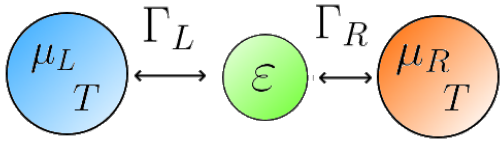

Figure 3.1: Schematic description of S.E.T model, ε is the energy of the quantum dot level, without loss of generality we will consider the case $\varepsilon = 0$.

The thermodynamics for this model is straight forward, defining $W > 0$ as useful work and $Q < 0$ as a heat flow from the reservoirs into the system, we have from the first law of thermodynamics

$$Q + W_{\text{chemical}} = 0. \tag{3.3}$$

Where W_{chemical} is the chemical energy gained from moving an electron between the different reservoirs, in the ideal case moving one electron from the left to the right reservoirs gives $W_{\text{chemical}} = \Delta\mu$, hence $W_{\text{chemical}} > 0$ would give us an engine that moves electrons from low chemical potential to high chemical potential using information, which gives a region where the system behaves as a classical Maxwell demon.

For this model the system Hamiltonian $\hat{H} = \varepsilon \left|1\right\rangle\!\left\langle 1\right|$ does not influence the system dynamics apart from the coherence present. However, the populations and coherence terms of the density matrix will turn out to be decoupled. Since we are mainly interested in the populations we will set $\varepsilon = 0$. What remains in the model is therefore the coupling to the left and right reservoirs and the system Liouvillian is then given by

$$\mathcal{L}(D) = \underbrace{\Gamma_L(D) f_L \mathcal{D}\left\{\left|1\right\rangle\!\left\langle 0\right|\right\} + \Gamma_L(D)(1-f_L)\mathcal{D}\left\{\left|0\right\rangle\!\left\langle 1\right|\right\}}_{\mathcal{L}_L(D)} + \underbrace{\Gamma_R(D) f_R \mathcal{D}\left\{\left|1\right\rangle\!\left\langle 0\right|\right\} + \Gamma_R(D)(1-f_R)\mathcal{D}\left\{\left|0\right\rangle\!\left\langle 1\right|\right\}}_{\mathcal{L}_R(D)}. \tag{3.4}$$

Here $\mathcal{L}_L(D)$ and $\mathcal{L}_R(D)$ are the coupling to the left and right reservoir respectivly. We include a D dependence on the tunneling rates to indicate that we will allow these rates to depend on the obtained measurement signal in order to implement the feedback. The Liouvillians $\mathcal{L}_L(D)$ and $\mathcal{L}_R(D)$ have the same structure, where the first term described the process of adding one electron to the dot with rate $\Gamma_i(D) f_i$, and the second term describes removing one electron from the dot with rate $\Gamma_i(D)(1-f_i)$, with f_i being the Fermi-Dirac distribution for reservoir $i = L, R$.

In general the density matrix for this problem can be written as

$$\rho = \begin{pmatrix} \rho_{00} & \rho_{01} \\ \rho_{10} & \rho_{11} \end{pmatrix}, \tag{3.5}$$

in the eigenbasis of σ_z, with $\rho_{11} + \rho_{00} = 1$ and $\rho_{01} = \rho_{10}^*$. It is convenient to vectorize the density matrix as

$$\rho \implies \begin{pmatrix} \rho_{00} & \rho_{01} & \rho_{10} & \rho_{11} \end{pmatrix}^T, \tag{3.6}$$

such that we can write the action of the superoperator $\mathcal{L}$ on ρ as a matrix operation with $\mathcal{L}(D)$ given by

$$\mathcal{L}(D) = \begin{pmatrix} -\Gamma_L f_L - \Gamma_R f_R & 0 & 0 & \Gamma_L(1-f_L) + \Gamma_R(1-f_R) \\ 0 & -\Gamma_L/2 - \Gamma_R/2 & 0 & 0 \\ 0 & 0 & -\Gamma_L/2 - \Gamma_R/2 & 0 \\ \Gamma_L f_L + \Gamma_R f_R & 0 & 0 & -\Gamma_L(1-f_L) - \Gamma_R(1-f_R) \end{pmatrix}. \tag{3.7}$$

The dissipator term in Eq.(2.39) becomes

$$\mathcal{D}[\sigma_z]\rho = \sigma_z \rho \sigma_z - \frac{1}{2}\{\sigma_z^2, \rho\} = \begin{pmatrix} 0 & -2\rho_{01} \\ -2\rho_{10} & 0 \end{pmatrix} \tag{3.8}$$

Or once again using vectorized ρ

$$\lambda\mathcal{D}[\sigma_z] = \begin{pmatrix} 0 & 0 & 0 & 0 \\ 0 & -2\lambda & 0 & 0 \\ 0 & 0 & -2\lambda & 0 \\ 0 & 0 & 0 & 0 \end{pmatrix} \tag{3.9}$$

(Note that this operator only acts on the off-diagonal elements of the density matrix, and since the diagonal and off-diagonal elements are decoupled, the system will in the long time limit be completely classical (meaning diagonal in ρ)).

Let's consider the time evolution of the coherences. We find the final rate equation for the coherences as

$$\dot{\rho}_c(t) = \begin{pmatrix} -2\lambda - \frac{1}{2}(\Gamma_L + \Gamma_R) & 0 \\ 0 & -2\lambda - \frac{1}{2}(\Gamma_L + \Gamma_R) \end{pmatrix} \rho_c(t) \tag{3.10}$$

with

$$\rho_c(t) = \begin{pmatrix} \rho_{01} & \rho_{10} \end{pmatrix}^T, \tag{3.11}$$

and the solution reads

$$\rho_{01}(t) = \rho_{01}(0)e^{-2\lambda t - \frac{1}{2}(\Gamma_L+\Gamma_R)t} \quad \rho_{10}(t) = \rho_{10}(0)e^{-2\lambda t - \frac{1}{2}(\Gamma_L+\Gamma_R)t} \tag{3.12}$$

The coherences of this system will decay to zero. Such that after some time (determined by the measurement strength and tunneling rates) the coherence's of the system will vanish and the classical and quantum version of the system are identical.

For the feedback scheme we will be turning on and off the left and right tunneling rates depending on some cutoff value for the measured signal. Since the ideal value of the detector for occupied and empty energy level is 1 and -1 respectivly it is natural to choose this cut-off as 0. We can then write the new system Liouvillian as

$$\mathcal{L}(D) = (1 - \Theta(D))\mathcal{L}_L + \Theta(D)\mathcal{L}_R. \tag{3.13}$$

Where $\Theta(D)$ is the Heaviside function.

3.2 Applying Separation of Timescales

We saw above that the time evolution of the coherence's and the populations are decoupled such that we can consider their time evolutions separately. We begin by considering the populations (diagonal terms of ρ). Let's begin by considering the diagonal terms of Eq.(2.47)

$$\dot{\rho}_p(t) = \int D'\mathcal{L}(D') \left(\sum_{a,a'} G_{a,a'}\mathcal{P}_{a,a'} \right) \rho(t) \tag{3.14}$$

We can write this as

$$\int dD' \begin{pmatrix} G_{00}(-\Gamma_L f_L(1-\Theta(D)) - \Gamma_R f_R \Theta(D)) & G_{11}(\Gamma_L(1-f_L)(1-\Theta(D) + \Gamma_R(1-f_R)\Theta(D)) \\ G_{00}(\Gamma_L f_L(1-\Theta(D)) + \Gamma_R f_R \Theta(D)) & G_{11}(-\Gamma_L(1-f_L)(1-\Theta(D)) - \Gamma_R(1-f_R)\Theta(D)) \end{pmatrix} \rho_p(t) \tag{3.15}$$

with

$$\rho_p = \begin{pmatrix} \rho_{00} & \rho_{11} \end{pmatrix}^T, \tag{3.16}$$

where G_{00} and G_{11} are the detector functions given by

$$G_{00/11}(D) = \sqrt{\frac{4\lambda}{\pi\gamma}} e^{-\frac{4\lambda}{\gamma}(D\pm 1))^2}. \tag{3.17}$$

Now it is only a matter of carrying out the integrations in Eq.(3.15). Performing this integration we end up with the result

$$\dot{\rho}_p(t) = \begin{pmatrix} -\Gamma_L f_L \kappa_1 - \Gamma_R f_R \kappa_2 & \Gamma_L(1-f_L)\kappa_2 + \Gamma_R(1-f_R)\kappa_1 \\ \Gamma_L f_L \kappa_1 + \Gamma_R f_R \kappa_2 & -\Gamma_L(1-f_L)\kappa_2 - \Gamma_R(1-f_R)\kappa_1 \end{pmatrix} \rho_p(t) \tag{3.18}$$

Where $2\kappa_1 = 1 + erf(\sqrt{4\lambda/\gamma})$ and $2\kappa_2 = 1 - erf(\sqrt{4\lambda/\gamma})$, such that $\kappa_1 + \kappa_2 = 1$, $erf(x)$ is the error function defined by

$$erf(x) = \frac{2}{\sqrt{\pi}} \int_0^x dx e^{x^2}. \tag{3.19}$$

Here κ_1 is interpreted as the probability to apply the correct feedback control given the state of the system, while κ_2 is then the probability to apply the incorrect feedback given the state of the system. Once again, since the populations does not couple to the coherences we arrive at the time evolution of the populations given by

$$\dot{\rho}_p(t) = \underbrace{\begin{pmatrix} -\Gamma_L f_L \kappa_1 - \Gamma_R f_R \kappa_2 & \Gamma_L(1-f_L)\kappa_2 + \Gamma_R(1-f_R)\kappa_1 \\ \Gamma_L f_L \kappa_1 + \Gamma_R f_R \kappa_2 & -\Gamma_L(1-f_L)\kappa_2 - \Gamma_R(1-f_R)\kappa_1 \end{pmatrix}}_{\mathcal{L}_p} \rho_p(t), \tag{3.20}$$

with solution

$$\rho_p(t) = e^{\mathcal{L}_p t}\rho_p(0), \tag{3.21}$$

where

$$e^{\mathcal{L}_p t} = \frac{1}{a+b}\begin{pmatrix} ae^{-(a+b)t} + b & -b(e^{-(a+b)t} - 1) \\ -a(e^{-(a+b)t} - 1) & -be^{-(a+b)t} + a \end{pmatrix} \tag{3.22}$$

with $a = \Gamma_L f_L \kappa_1 + \Gamma_R f_R \kappa_2$ and $b = \Gamma_L(1-f_L)\kappa_2 + \Gamma_R(1-f_R)\kappa_1$. The steady-state solutions are given by

$$\rho_{00} = \frac{b}{a+b}, \quad \rho_{11} = \frac{a}{a+b}. \tag{3.23}$$

Note that the only way that the effect of the feedback protocol enters are through κ_1.

3.3 S.E.T with counting field

Let us now introduce a counting field for the electrons going into the right reservoir. The new Liouvillian then becomes (see discussion of counting fields in section 2.8).

$$\dot{\rho}_p(t) = \underbrace{\begin{pmatrix} -\Gamma_L f_L \kappa_1 - \Gamma_R f_R \kappa_2 & \Gamma_L(1-f_L)\kappa_2 + \Gamma_R(1-f_R)\kappa_1 e^{i\chi} \\ \Gamma_L f_L \kappa_1 + \Gamma_R f_R \kappa_2 e^{-i\chi} & -\Gamma_L(1-f_L)\kappa_2 - \Gamma_R(1-f_R)\kappa_1 \end{pmatrix}}_{\mathcal{L}_p(\chi)} \rho_p(t). \tag{3.24}$$

From this we can then find the steady state current I using (See section 2.8)

$$I = \lim_{t\to\infty} \langle \dot{n}(t) \rangle = -i \operatorname{Tr}\{\mathcal{L}'(0)\rho_{ss}\}. \tag{3.25}$$

We also want to consider the ratio of the current and the current fluctuations i.e $\mathcal{Q} = \frac{I}{\Delta I}$, with ΔI given by (see section 2.8)

$$\Delta I \approx -\lambda''(0). \tag{3.26}$$

$\mathcal{Q}$ gives information about the correlations in the transport and of the size of fluctuations in the transport. $\mathcal{Q}$ is referred to as the inverse Fano-Factor. Performing the calculations using the Liouvillan given in equation 3.24 we arrive at

$$I = \Gamma_L \Gamma_R \left[\frac{f_L \kappa_1 (1-f_R)\kappa_1 - f_R \kappa_2 (1-f_L)\kappa_2}{\Gamma_L f_L \kappa_1 + \Gamma_R f_R \kappa_2 + \Gamma_L(1-f_L)\kappa_2 + \Gamma_R(1-f_R)\kappa_1} \right] = \frac{\gamma_1\gamma_4 - \gamma_2\gamma_3}{\sum_i \gamma_i}, \tag{3.27}$$

$$\Delta I = \frac{2(\gamma_2\gamma_3 - \gamma_1\gamma_4)^2 - (\gamma_1\gamma_4 + \gamma_2\gamma_3)(\gamma_1 + \gamma_2 + \gamma_3 + \gamma_4)^2}{\left(\sum_j \gamma_j\right)^3}, \tag{3.28}$$

with

$$\begin{aligned} \gamma_1 &= \Gamma_L f_L \kappa_1; & \gamma_2 &= \Gamma_R f_R \kappa_2 \\ \gamma_3 &= \Gamma_L(1-f_L)\kappa_2; & \gamma_4 &= \Gamma_R(1-f_R)\kappa_1. \end{aligned} \tag{3.29}$$

We quickly note that the result in 3.27 have a nice interpretation. The numerator contains two opposing currents, one going from the left reservoir to the right and one current going the other way around. Remember that κ_1 is the probability to apply the correct feedback control given the state of the system while κ_2 is the probability to apply the incorrect feedback. Hence, we can interpret the first term as correctly opening the left "valve" followed by correctly opening the right valve, resulting in a current from left to right. While the second term is the probability to wrongly opening the right valve followed by wrongly opening the left valve, giving a current in the opposing direction.

3.4 Analytical Results

We can now examine the behaviour of the current depending on the parameters on the system and look at the current and inverse Fano-Factor $\mathcal{Q}$ as a function of λ/γ for some values of $\Delta\mu/k_bT$. We will also consider the power production generated from moving electrons from one chemical potential to another.

From figures 3.2 and 3.3 it is seen that as the measurement strength increases (i.e $\lambda \to \infty$) meaning that as the probability to perform the wrong feedback operation tends to zero, the resulting steady state current becomes maximal. It is also noted that as $\Delta\mu$ increases the maximum steady state current decreases, for positive $\Delta\mu$ the current starts out as negative for λ/γ equal to zero, meaning that no meaningful feedback is performed (the controller is randomly sampling between the two feedback options). The result of this is that the current flow from high to low chemical potential, as is expected if the system is left on its own without applying any feedback. We see that as the accuracy of the detector goes up it is possible to reverse the direction of this current and move electrons from low to high chemical potential. Since this current is against the applied bias this indicates a region were the systems acts as a Maxwell demon. Hence, with sufficiently strong measurements it is possible to convert the information gained of the state of the system into chemical work.

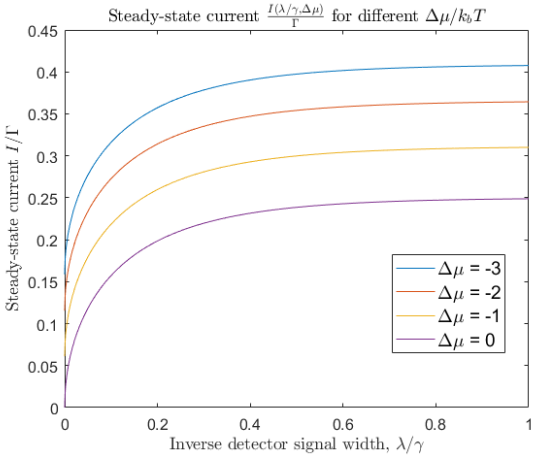

Figure 3.2: Steady-State current as a function of λ/γ for a couple different values of $\Delta\mu \leq 0$.

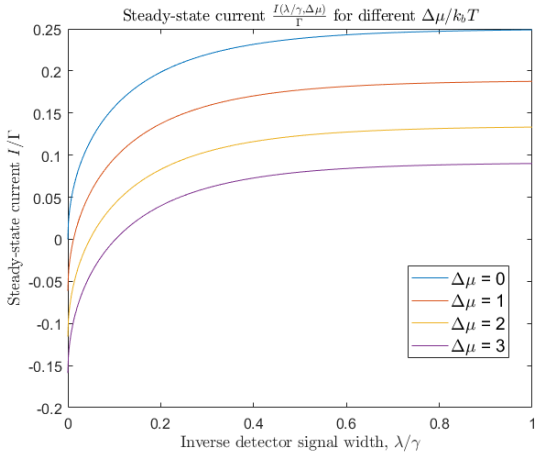

Figure 3.3: Steady-State current as a function of λ/γ for a couple different values of $\Delta\mu \geq 0$.

For the fluctuations of the current it is seen from figure 3.4 and figure 3.5 that the fluctuations in the current drastically decreases for increasing λ/γ and approaches a limiting value of 0.5. This is implying that there is a minimum amount of fluctuations achievable that is at least half of the steady state current. It is also noted that the convergence to this limiting value becomes slower for larger $\Delta\mu$ implying that when trying to reverse the current flow against the direction dictated by the chemical potential gradient, a larger amount of fluctuation in the resulting current is obtained that in turn can be reduced by increasing the strength of the measurement, thus increasing the accuracy of the detector.

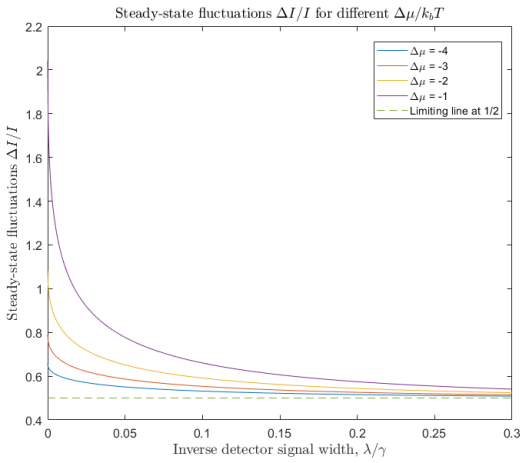

Figure 3.4: Steady-State current fluctuations as a function of λ/γ for a couple different values of $\Delta\mu \leq 0$.

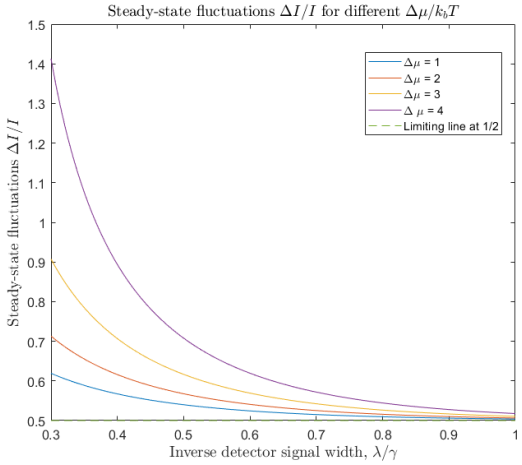

Figure 3.5: Steady-State current fluctuations as a function of λ/γ for a couple different values of $\Delta\mu \geq 0$.

The power production for the system can be seen in figure 3.6, the red lines indicate where the power production is zero and divide the parameter space into two regions where the system acts as a Maxwell demon and a region where the current follows what is dictated by thermodynamics. There seems to be diminishing returns when considering larger chemical potential differences, for this particular choice of parameters there is a maximum in the power production at $\Delta\mu \approx 2.5 k_B T$.

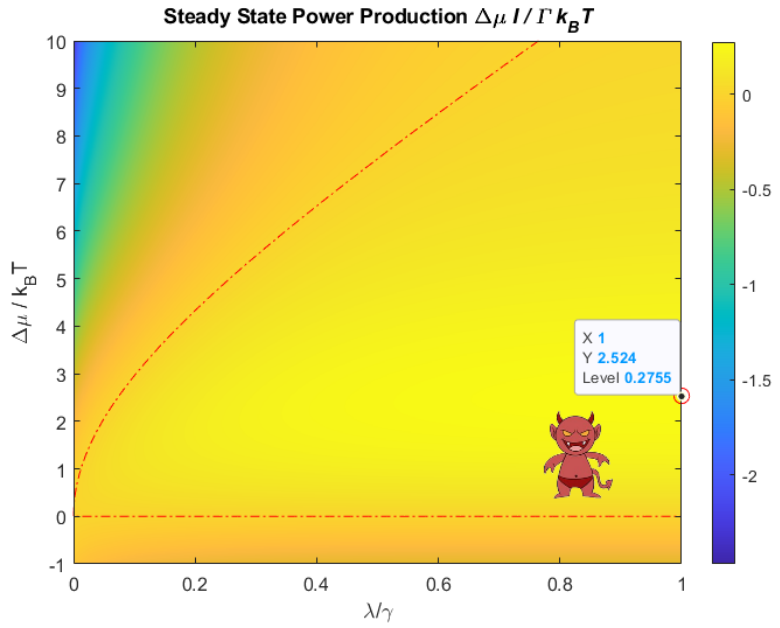

Figure 3.6: Steady-state power generation as a function of λ/γ and $\Delta\mu$, The red lines are contour lines for zero power production, the inscribed triangular region corresponds to parameter values were the system acts as a Maxwell demon. Maximum power production is also shown.

3.5 Numerics

Here, we solve the QFPME (Eq.(2.39)) for the system numerically, and compare the results with the separation of timescales approximation. The comparison is made for the steady state detector distribution function $P(D)$ as well as the obtained current. For all the cases 300 polynomials where used in the series expansion. Details about this particular implementation of the numerics can be found in the appendix 6.2.1 and in sec. 2.9.

3.6 Numerics Results

We begin by considering symmetric tunneling i.e $\Gamma_L = \Gamma_R = \Gamma$, we further set $f_L = f_R = 1/2$ and $\gamma/8\lambda = 0.05$. From the plots showing the detector distribution function in steady state (figures 3.7a to 3.7f) it is observed that for small values of Γ/γ the full numerical solution and the solution assumed using separation of timescales agree very well, while the error between the correct numerical solution and the separation of timescales approximation grows as the ratio Γ/γ grows. In the symmetric case the approximation seems hold quite well up to $\Gamma/\gamma \approx 0.1$. What is more interesting is that the ratio γ/λ determined by σ does not seem to influence how well the approximation behaves. The value of σ can be made very small (as in the plots below) and there is still a very good agreement with the separation of timescales approximation even though small $\sigma < 1$ is formally outside the region where separation of timescales holds. This implies that measurement back-action does not directly influence the dynamics. The value of λ compared to γ does not matter as much. It is mainly the relation of Γ to γ that influences the accuracy of the approximation.

We note that in figure 3.7f it is seen that for regions were the dynamics of the system is quick compared to the dynamics of the detector the ability to distinguish between the two states vanishes. Implying that for large ratios Γ/γ no meaningful feedback can be performed since the detector loses the ability to distinguish between the two states.

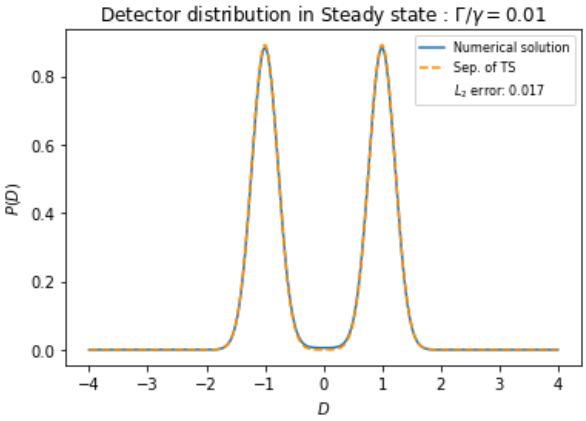

(a)

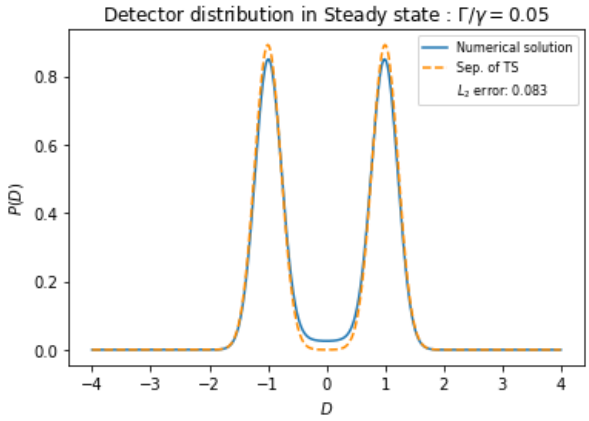

(b)

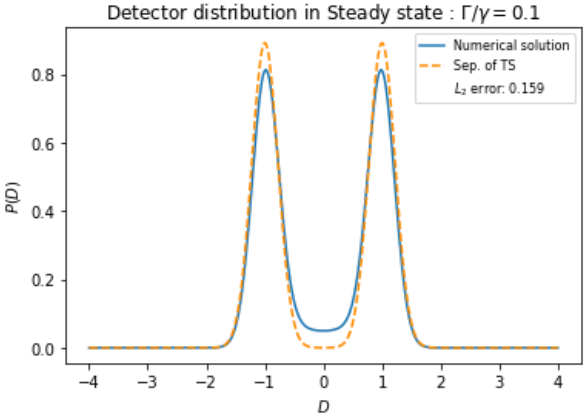

(c)

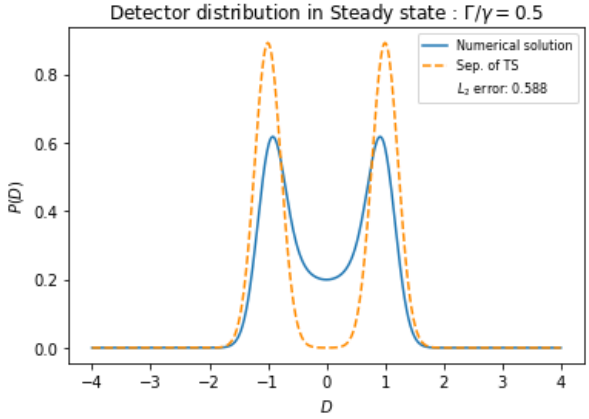

(d)

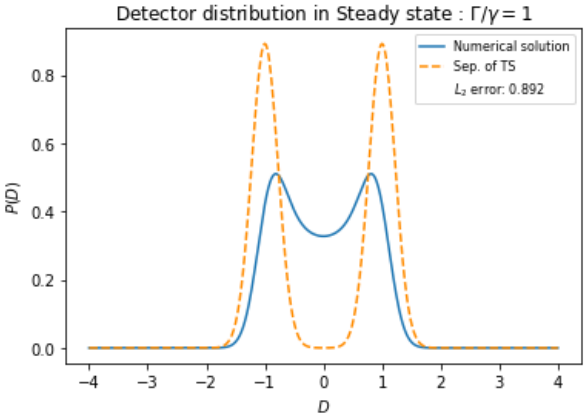

(e)

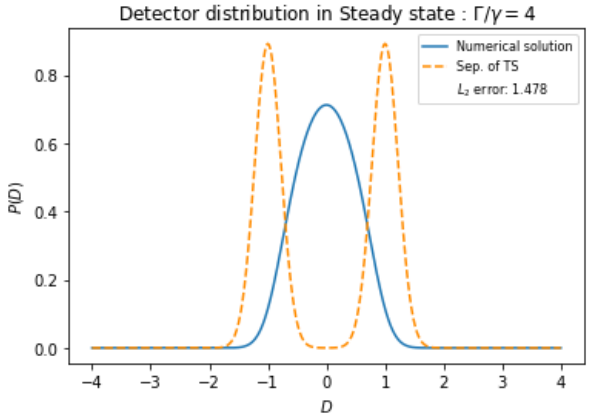

(f)

Figure 3.7: Detector distribution function at steady state. Results are for symmetric tunneling $\Gamma_L = \Gamma_R = \Gamma$ and $f_L = f_R = 1/2$ with $\gamma/8\lambda = 0.05$. a) to f)is increasing Γ/γ, the discrepancy between the analytics and numerics increases with increasing Γ/γ.

We also consider the asymmetric tunneling case (shown in figures 3.8a-3.8f). Here similar results are obtained and the separation of timescales and full numeric solution agree very well up to around $\Gamma/\gamma \approx 0.1$. We investigated $\Gamma_L/2 = \Gamma_R = \Gamma$ and $f_L = f_R = 1/2$ with $\gamma/8\lambda = 0.05$. The obtained L_2 error between the full numerical and the result obtained from the separation of timescales approximation grow faster in the asymmetric case, when comparing equal values of Γ/γ for the symmetric and asymmetric case. Otherwise the results agree very well. Also in this case the detector loses the ability to distinguish between occupied and unoccupied dot for values of $\Gamma/\gamma > 1$ even for the asymmetric case, which might indicate that problems with applying the separation of timescales approximation might occur when the tunneling is strongly asymmetric. However, the difference is still quite small and might be a result of numerical error.

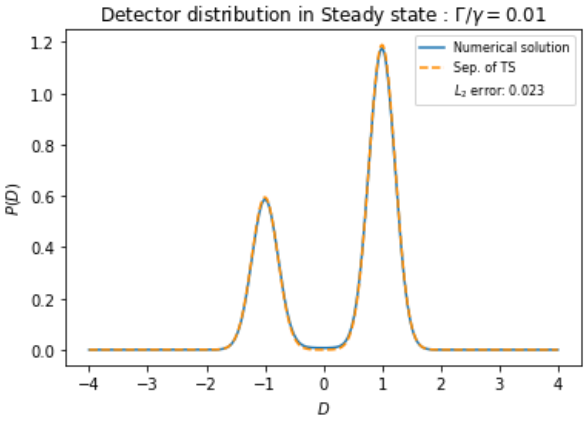

(a)

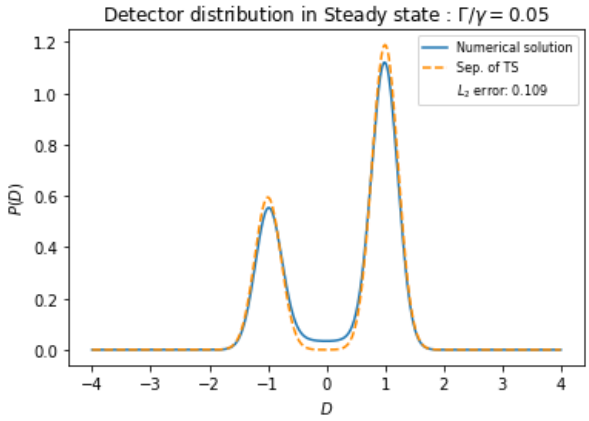

(b)

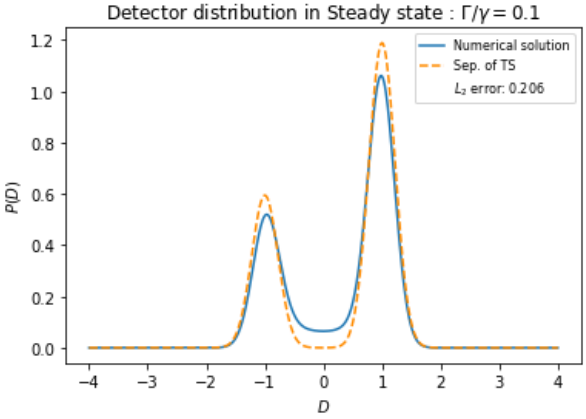

(c)

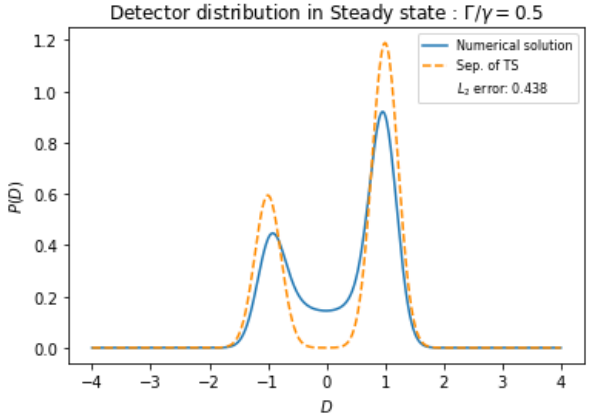

(d)

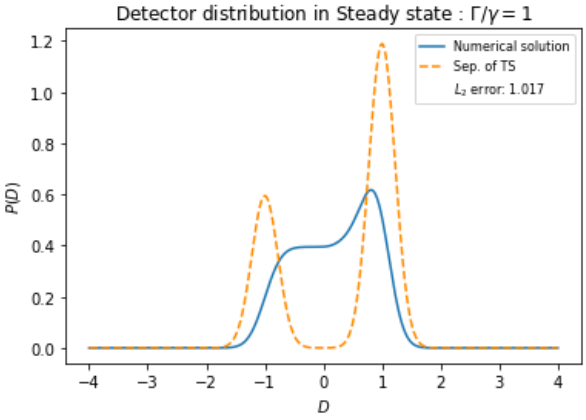

(e)

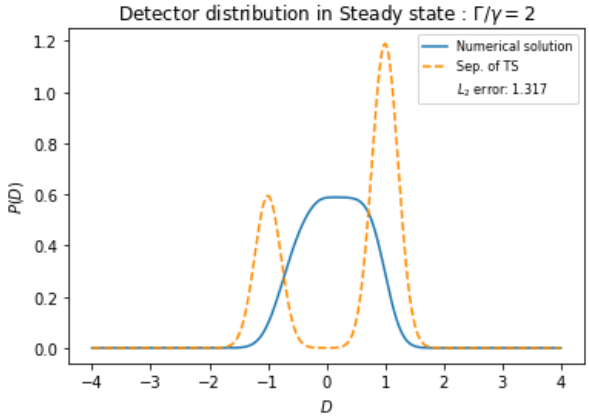

(f)

Figure 3.8: Detector distribution function at steady state, Asymmetric tunneling case with $\Gamma_L/2 = \Gamma_R = \Gamma$ and $f_L = f_R = 1/2$ with $\gamma/8\lambda = 0.05$. a) to f)is increasing Γ/γ. Similar results compared to the symmetric tunneling case is observed. The discrepancy between the analytics and numerics increases with increasing Γ/γ.

We now consider the current through the system for different applied chemical biases. Setting $\Gamma_L = \Gamma_R = \Gamma$ but considering the current as a function of Γ/λ. It was above seen that as the timescale of the system compared to the detector delay (Γ/γ) grows, the feedback controller looses the ability to resolve the two states, and the detector distribution function becomes more and more centered around $D = 0$. The fact that the controller looses the ability to react fast enough compared to the system timescale is also seen when looking at the current plots (figures 3.9a - 3.9d). For small values of Γ/γ the full numerical solution and the result obtained from the separation of timescales approximation agrees very well as is expected. When the ratio Γ/γ is increased the current into the right reservoir is reduced representing the fact that the feedback controller looses the ability to react fast enough in order to perform correct feedback actions and as a result the current achived is reduced.

It is also noted that as the applied chemical potential bias $\Delta\mu$ is increased, the difference between the numerical and analytical result for larger values of Γ/γ shrinks, implying that if the chemical bias is too strong there is too strong of a tendency for the system to move in the opposite direction compared to the current direction that the feedback controller is aiming for. Hence, if the chemical bias is made large the actual timescale of the system compared with the detector becomes less important. However, it is clearly seen in figure 3.9d that for high chemical bias that larger Γ/γ does no longer agree with the separation of timescale result even for small λ/γ

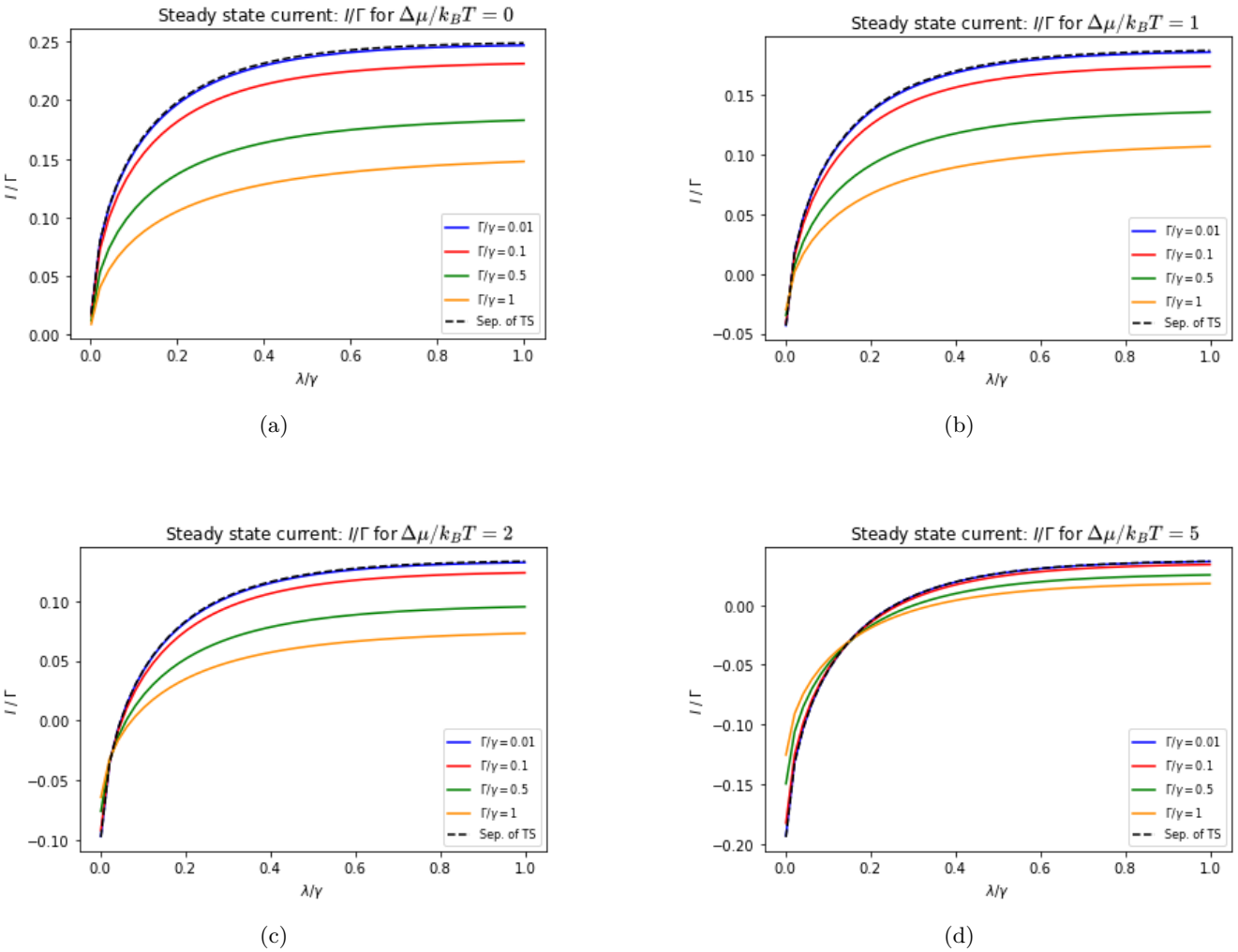

(a) (b)

(c) (d)

Figure 3.9: Steady state current for different values of $\Delta\mu/k_bT$ and ratios Γ/γ, solid lines are numerical results, dotted line is result from separation of timescales It is noted that small Γ/γ agree very well with separation of timescales approximation, the spread in the numerical and analytical results decreases as $\Delta\mu$ increases.

Chapter 4

Quantum system - Double Dot

We now turn our attention to a fully quantum model, namely a double dot system consisting of two single level quantum dots that are coherently coupled. This is a quantum version of the system considered in [37], and is of interest since experimental studies on such a system is scheduled to take place at the NanoLund center at Lund University in the later part of 2022. The goal of the following analysis is to investigate the properties of the transport in such a system using a certain feedback scheme. We will investigate whether or not it is possible to implement a quantum Maxwell demon using the proposed feedback scheme.

4.1 Model & Feedback scheme

Below in figure 4.1 a simplified visualization of the model. The quantum dots are coupled to two fermionic reservoirs via tunneling rates Γ_L and Γ_R. The reservoirs have the same temperature T, but different chemical potentials μ_L and μ_R. The dots have tunable energy levels given by ε_L and ε_R and a coupling between them given by the coupling constant g.

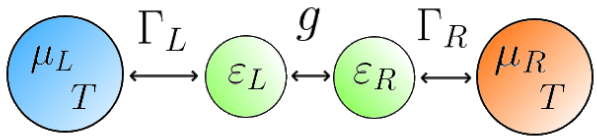

Figure 4.1: Schematic description of transport in model with a double quantum dot with energy levels ε_L and ε_R.

In figure 4.2 a more detailed description of the model is presented, where the different settings of the energies of $|L\rangle$ and $|R\rangle$ are shown. The model only considers the states $|0\rangle$, $|L\rangle$ and $|R\rangle$, corresponding to having no electron in the levels, as well as having one electron at any of the two energy levels. We do not consider states such as $|LR\rangle$ where both energy levels are occupied since it is assumed that there is a suffiently strong inter-dot Coulomb repulsion present, making it impossible of having both islands occupied at the same time. Furthermore, it is assumed that there is no coherence present between $|0\rangle$ and $|L\rangle$ or$|R\rangle$ since it is assumed that as soon as an electron makes the jump into either the left or right reservoir all coherence with the rest of the system is killed by the strong interaction with the rest of the reservoir. With these assumptions stated the general density matrix for this problem can be

written (in the $\{|0\rangle, |L\rangle, |R\rangle\}$ basis) as

$$\rho = \begin{pmatrix} \rho_{00} & 0 & 0 \\ 0 & \rho_{LL} & \rho_{LR} \\ 0 & \rho_{LR}^* & \rho_{RR} \end{pmatrix}. \tag{4.1}$$

The model Hamiltonian is given by

$$\hat{H} = \begin{pmatrix} 0 & 0 & 0 \\ 0 & \varepsilon_L(D) & g \\ 0 & g & \varepsilon_R(D) \end{pmatrix}. \tag{4.2}$$

For the coupling to the reservoirs the following is considered

$$\mathcal{L}_{env}(D) = \mathcal{L}_L(D) + \mathcal{L}_R(D). \tag{4.3}$$

With

$$\mathcal{L}_L(D) = \Gamma_L f_L(\varepsilon_L(D))\mathcal{D}\{|L\rangle\langle 0|\} + \Gamma_L(1 - f_L(\varepsilon_L(D))\mathcal{D}\{|0\rangle\langle L|\} \tag{4.4}$$

and

$$\mathcal{L}_R(D) = \Gamma_R f_R(\varepsilon_R(D))\mathcal{D}\{|R\rangle\langle 0|\} + \Gamma_R(1 - f_R(\varepsilon_R(D)))\mathcal{D}\{|0\rangle\langle R|\}. \tag{4.5}$$

Where the dependence on the detector signal D have been included in the Fermi functions of the two reservoirs, as a reminder that the feedback scheme will consist of shifting the energy levels of the two dots. Vectorising the density matrix as

$$\rho = \begin{pmatrix} \rho_{00} & \rho_{LL} & \rho_{RR} & \rho_{LR} & \rho_{RL} \end{pmatrix}^T, \tag{4.6}$$

gives total system matrix for the double dot system as

$$\mathcal{L}_{\text{tot}}(D) = \begin{pmatrix} -\gamma_L - \gamma_R & \bar{\gamma}_L & \bar{\gamma}_R & 0 & 0 \\ \gamma_L & -\bar{\gamma}_L & 0 & ig & -ig \\ \gamma_R & 0 & -\bar{\gamma}_R & -ig & ig \\ 0 & ig & -ig & -i\Delta\varepsilon - \frac{\bar{\gamma}_L + \bar{\gamma}_R}{2} & 0 \\ 0 & -ig & ig & 0 & i\Delta\varepsilon - \frac{\bar{\gamma}_L + \bar{\gamma}_R}{2} \end{pmatrix}. \tag{4.7}$$

With

$$\gamma_{L/R}(D) = \Gamma_{L/R} f(\varepsilon_{L/R}(D)),\ \ \bar{\gamma}_{L/R}(D) = \Gamma_{L/R}(1 - f(\varepsilon_{L/R}(D)))\ \text{ and }\ \Delta\varepsilon(D) = \varepsilon_L(D) - \varepsilon_R(D). \tag{4.8}$$

The feedback scheme considered will consist of moving the energy levels corresponding to $|L\rangle$ and $|R\rangle$ depending on a measurement signal D. The scheme considers three positions of the energy levels: ε_0 (perfectly in between μ_L and μ_R) and an up-shifted position ε_u and a downshifted position ε_d. These are shown in figure 4.2. The feedback operation contains three steps that are outlined in figure 4.3.

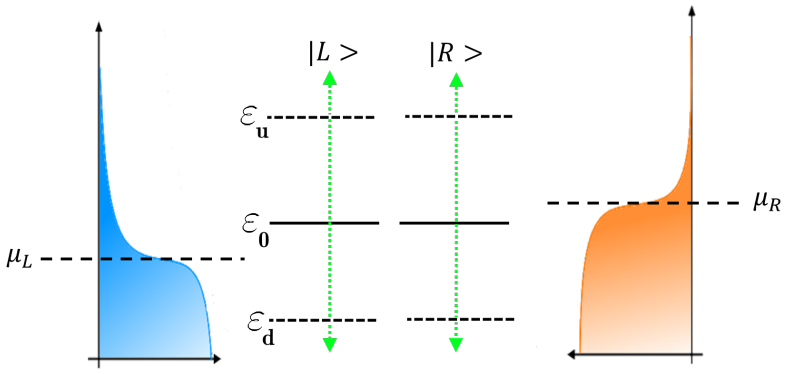

Figure 4.2: A more detailed description of the double dot system, showing the different possible settings of the energy levels ε_L and ε_R.

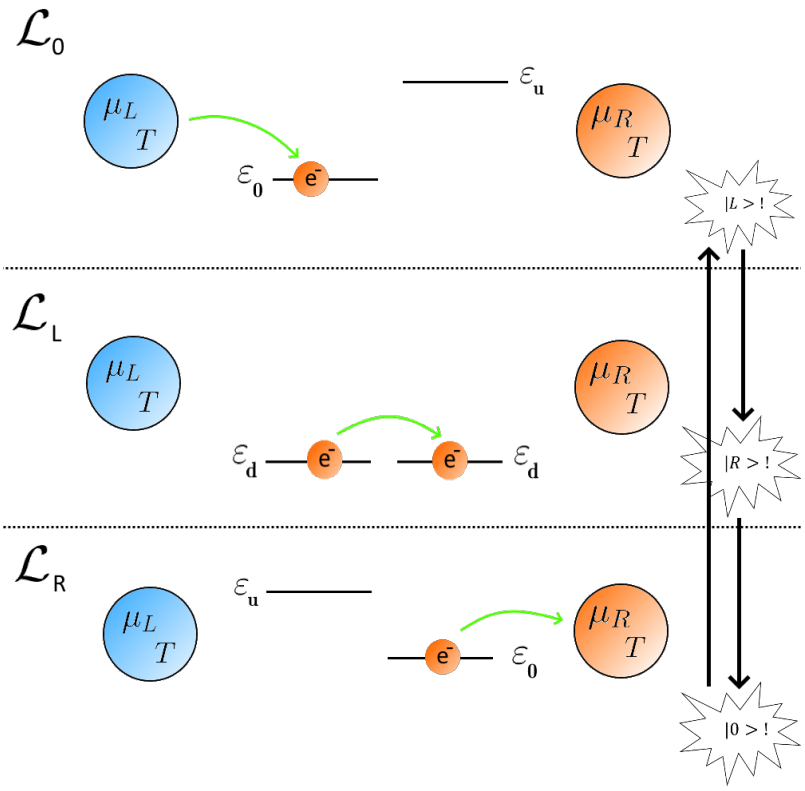

Figure 4.3: Feedback scheme considered for the Double Dot system. As soon as the detector detects an electron in $|L\rangle$ (top panel) the energy levels are instantaneously moved down to ε_d (middle panel). Once the detector then detects and electron in the $|R\rangle$ state the right energy level is moved to ε_0 while the left energy level is moved up to ε_u (bottom panel). Once the detector then detects the system as being empty of electrons the energy levels are moved to the original setting (top panel) and the process starts over again. This represents one ideal cycle of operation.

The first step in the feedback scheme is given by $\mathcal{L}_0$ in the top most panel of figure 4.3. Here the left energy level is moved into the middle position while the right level is moved up to ε_u in order to stop tunneling in from the right reservoir. Once an electron have jumped into the left energy level and the detector detects the left level as being filled, the two energy levels are instaneously moved to ε_d and $\mathcal{L}_L$ is applied. Since the left energy should be filled at this point and due to the assumed Coulomb repulsion for the inter-dot interaction no transport between the reservoirs and the levels should occur at this point. The coherent coupling between the levels will then cause the state $|R\rangle$ to be populated. Once the detector detects an electron in the right state the energy levels are then moved into a flipped position compared to the starting state, namely the right energy level is now positioned at the middle position and the left energy level is moved into the ε_u position and $\mathcal{L}_R$ is applied. Finally, once the detector detects the levels as empty the levels are moved back to the starting position and $\mathcal{L}_0$ is applied again.

The thermodynamics of one cycle of operation is then given by

$$Q + W_{\text{levels}} + W_{\text{chemical}} = 0. \tag{4.9}$$

Here useful work is defined as $W > 0$, Q is the heat released from the reservoirs into the system, $Q < 0$ is considered as a net heat flow into the system. W_{chemical} is the chemical work gained from moving electrons from one chemical potential to another, W_{levels} is the work put into the system when moving the energy levels with an electron on them. For each electron that is transported from the left to the right reservoir there is a gain in the chemical work given by $\Delta\mu = \mu_R - \mu_L$. W_{levels} should ideally be zero since during one ideal cycle the following holds $W_{\text{levels}} = (\varepsilon_d - \varepsilon_0) + (\varepsilon_0 - \varepsilon_d) = 0$. However, this is assuming that there are no feedback errors present.

So in order for the system to function as a Maxwell demon and not only a electron pump, the gain from the chemical work must exceed the energy put in by moving the levels i.e

$$W_{\text{chemical}} > W_{\text{levels}}. \tag{4.10}$$

In general there are 6 possible transport channels possible for an electron entering or leaving the system (figure 4.4)

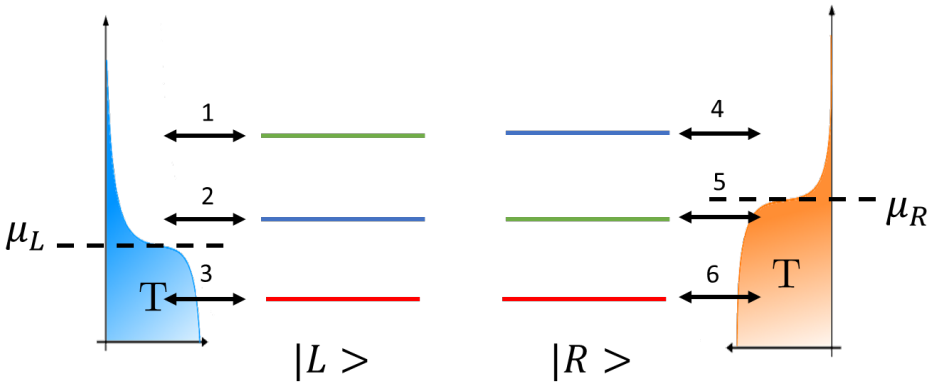

Figure 4.4: Schematic description of the classical transport channels in the model. The levels are color coded according to which Liouvillian they correspond to. The blue levels correspond to $\mathcal{L}_0$ being applied, red correspond to $\mathcal{L}_L$ being applied. Finally, green correspond to $\mathcal{L}_R$ being applied.

For optimal operation the electrons should only enter into the system through channel 2 and exit the right reservoir through channel 5 (corresponding to moving into the system when the left energy level is at ε_0 and leaving the system when the right energy level is also at ε_0). All other transport corresponds to unwanted currents for the purposes of this thesis ($W_{\text{levels}} \neq 0$) and will be considered error-currents. The number of transport channels are quite large. Fortunately it is possible to simplify the transport by choosing the values of the energy levels

appropriately, in such a way some of these channels will close. If ε_u is chosen such that $\varepsilon_u \gg \mu_L, \mu_R$ one can then safely assume that $f_{L/R}(\varepsilon_u) = 0$, similarly by choosing $\varepsilon_d \ll \mu_L, \mu_R$ we can also assume that $f_{L/R}(\varepsilon_d) = 1$.

Since the transition rates to go from a reservoir into the system when either of them is at ε_u is proportional to $f_{L/R}(\varepsilon_u)$, this assumption removes 2 transport channels. Similarly since moving out into the reservoirs when both levels are at ε_d is proportional to $1 - f_{L/R}(\varepsilon_d)$ these transport processes are also removed under this assumption. The rest of the error currents will turn out to depend on the accuracy of the detector involved.

4.2 Topological Error

In principle it would be possible to choose the measurement operator as

$$\sigma_m = \begin{pmatrix} 0 & 0 & 0 \\ 0 & -1 & 0 \\ 0 & 0 & 1 \end{pmatrix}, \tag{4.11}$$

such that the detector output 0 means the system is in state $|0\rangle$ and outputs -1 and 1 means the system are in states $|L\rangle$ and $|R\rangle$, respectivly. However, since the measurement signal is continuous this could lead to unwanted feedback problems due to the fact that in order for the system to move from feedback state $|L\rangle$ to $|R\rangle$, the system must pass through 0, meaning that the feedback controller could erroneously choose to apply feedback for the state $|0\rangle$, see Fig (4.5) and (4.6).

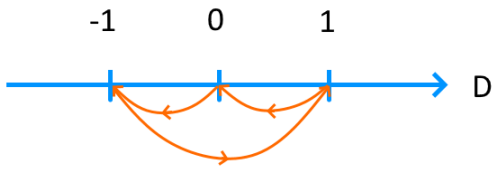

Figure 4.5: Operation cycle of protocol described above, note that the detector have to pass zero twice.

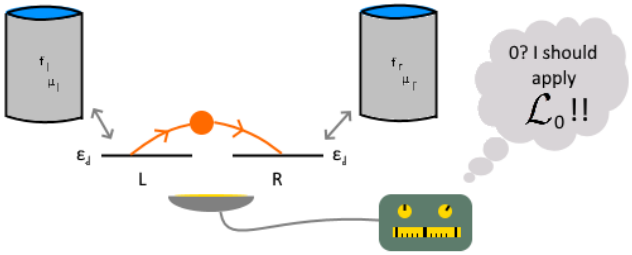

Figure 4.6: Demonstration that troubles determining the correct feedback action occurs because the operation cycle crosses itself in detector space.

It is possible to avoid this problem by instead considering two detectors, with measurement operators σ_1 and σ_2

$$\sigma_1 = \begin{pmatrix} 1 & 0 & 0 \\ 0 & -1 & 0 \\ 0 & 0 & -1 \end{pmatrix} \quad \text{and} \quad \sigma_2 = \begin{pmatrix} 0 & 0 & 0 \\ 0 & -1 & 0 \\ 0 & 0 & 1 \end{pmatrix}. \tag{4.12}$$

Note that $[\sigma_1, \sigma_2] = 0$. The first detector given by σ_1 only measures whether or not there is any electron present in the system, i.e the total charge of the system. This measurement does not give any information about whether the electron is in the state $|L\rangle$ or $|R\rangle$ and hence turns out to not influence the coherence of the systems through a back-action term, this is seen by

$$\lambda_1 \mathcal{D}[\sigma_1]\rho = 0. \tag{4.13}$$

Hence, the purely classical measurement given by σ_1 does not affect the dynamics of the system. Performing the same calculation for the second measurement (σ_2) and vectorizing ρ the following is obtained

$$\lambda_2 \mathcal{D}[\sigma_2]\rho = -2\lambda_2 \begin{pmatrix} 0 & 0 & 0 & 0 & 0 \\ 0 & 0 & 0 & 0 & 0 \\ 0 & 0 & 0 & 0 & 0 \\ 0 & 0 & 0 & 1 & 0 \\ 0 & 0 & 0 & 0 & 1 \end{pmatrix} \rho. \tag{4.14}$$

With these two measurements in conjunction the new ideal operation cycle can be pictured in detector space as in figure 4.7.

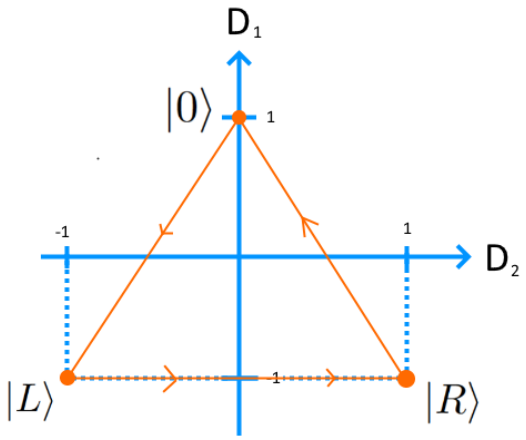

Figure 4.7: Operation cycle of topologically sound protocol. With the above choice of measurement operators the points (1,0), (-1,-1) and (1,-1) in $D_1 \times D_2$ ideally correspond to the system being in states $|0\rangle$, $|L\rangle$ and $|R\rangle$.

The feedback Liouvillian for the two measurements is given by

$$\mathcal{L}(D_1, D_2) = \mathcal{L}_0\Theta(D_1) + \mathcal{L}_L\Theta(-D_1)\Theta(-D_2) + \mathcal{L}_R\Theta(-D_1)\Theta(D_2). \tag{4.15}$$

Since the measurement operators are commuting, their effects are added separately into the general master equation, which gives the new master equation:

$$\partial_t\rho(t, D_1, D_2) = \mathcal{L}(D_1, D_2)\rho + \underbrace{\lambda_1 \mathcal{D}[\sigma_1]\rho}_{=0} + \lambda_2 \mathcal{D}[\sigma_2]\rho - \gamma_1\partial_{D_1}\mathcal{A}(D_1)\rho - \gamma_2\partial_{D_2}\mathcal{A}(D_2)\rho + \frac{\gamma_1^2}{8\lambda_1}\partial_{D_1}^2\rho + \frac{\gamma_2^2}{8\lambda_2}\partial_{D_2}^2\rho. \tag{4.16}$$

There are several ways to motivate this form. The simplest one is to go back to the derivation of the master equation where it is seen that with two commuting measurement operators one can perform the Taylor expansion of $\mathcal{M}(D_1, D_2|D_1', D_2') = \mathcal{M}(D_1|D_1')\mathcal{M}(D_2|D_2')$ independently and hence to first order in δt end up with the master equation with two measurement operators as given in equation 4.16 above.

4.3 Applying Separation of Timescales

We now apply the separation of timescales approximation for the double dot system in order to find analytical expressions for the transport properties.

A natural new ansatz for the separation of timescales with two detectors then becomes

$$\rho(D_1, D_2, t) = \sum_{a,a'} G^{(1)}_{a,a'}(D_1) G^{(2)}_{a,a'}(D_2) \rho_{a,a'} \left|a\right\rangle\!\left\langle a'\right| . \tag{4.17}$$

With detector functions for the classical detector (D_1) given by:

$$G^{(1)}_{00} = \sqrt{\frac{4\gamma}{\pi\lambda}} e^{\frac{-4\lambda}{\gamma}(D_1-1)^2},\ G^{(1)}_{LL} = \sqrt{\frac{4\gamma}{\pi\lambda}} e^{\frac{-4\lambda}{\gamma}(D_1+1)^2},\ G^{(1)}_{RR} = G^{(1)}_{LL},\ G^{(1)}_{LR} = G^{(1)}_{RL} = G^{(1)}_{LL}. \tag{4.18}$$

And for the D_2 detector:

$$G^{(2)}_{00} = \sqrt{\frac{4\gamma}{\pi\lambda}} e^{\frac{-4\lambda}{\gamma}D_2^2},\ G^{(2)}_{LL} = \sqrt{\frac{4\gamma}{\pi\lambda}} e^{\frac{-4\lambda}{\gamma}(D_2+1)^2},\ G^{(2)}_{RR} = \sqrt{\frac{4\gamma}{\pi\lambda}} e^{\frac{-4\lambda}{\gamma}(D_2-1)^2},\ G^{(2)}_{LR} = G^{(2)}_{RL} = G^{(2)}_{00}. \tag{4.19}$$

After applying the separation of timescales approximation an effective Liouvillian is obtained, given by

$$\mathcal{L}_{S.o.T} = \begin{pmatrix} -\gamma_1-\gamma_2 & \gamma_3 & \gamma_4 & 0 & 0 \\ \gamma_1 & -\gamma_3 & 0 & ig & -ig \\ \gamma_2 & 0 & -\gamma_4 & -ig & ig \\ 0 & ig & -ig & -i\alpha - \frac{\gamma_5+\gamma_6}{2} - 2\lambda_2 & 0 \\ 0 & -ig & ig & 0 & i\alpha - \frac{\gamma_5+\gamma_6}{2} - 2\lambda_2 \end{pmatrix}. \tag{4.20}$$

Without any further approximations being applied the rescaled constants are given by

$$\begin{aligned}
\gamma_1 &= \Gamma_L \left(f_L(\varepsilon_0)\kappa^{(1)}_1 + f_L(\varepsilon_l)\kappa^{(1)}_2/2 + f_L(\varepsilon_u)\kappa^{(1)}_2/2 \right), \\
\gamma_2 &= \Gamma_R \left(f_R(\varepsilon_u)\kappa^{(1)}_1 + f_R(\varepsilon_l)\kappa^{(1)}_2/2 + f_R(\varepsilon_0)\kappa^{(1)}_2/2 \right), \\
\gamma_3 &= \Gamma_L \left((1-f_L(\varepsilon_0))\kappa^{(1)}_2 + (1-f_L(\varepsilon_l))\kappa^{(1)}_1\kappa^{(2)}_1 + (1-f_L(\varepsilon_u))\kappa^{(1)}_1\kappa^{(2)}_2 \right), \\
\gamma_4 &= \Gamma_R \left((1-f_R(\varepsilon_u))\kappa^{(1)}_2 + (1-f_R(\varepsilon_l))\kappa^{(1)}_1\kappa^{(2)}_2 + (1-f_R(\varepsilon_0))\kappa^{(1)}_1\kappa^{(2)}_1 \right), \\
\gamma_5 &= \Gamma_L \left((1-f_L(\varepsilon_0))\kappa^{(1)}_2 + (1-f_L(\varepsilon_l))\kappa^{(1)}_1/2 + (1-f_L(\varepsilon_u))\kappa^{(1)}_1/2 \right), \\
\gamma_6 &= \Gamma_R \left((1-f_R(\varepsilon_u))\kappa^{(1)}_2 + (1-f_R(\varepsilon_l))\kappa^{(1)}_1/2 + (1-f_R(\varepsilon_0))\kappa^{(1)}_1/2 \right), \\
\alpha &= (\varepsilon_0-\varepsilon_u)\kappa^{(1)}_2 + (\varepsilon_u-\varepsilon_0)\frac{\kappa^{(1)}_1}{2}.
\end{aligned} \tag{4.21}$$

Further applying the idealized situation $f_{L/R}(\varepsilon_d) = 1$ and $f_{L/R}(\varepsilon_u) = 0$, the following is obtained

$$\gamma_1 = \Gamma_L \left(f_L(\varepsilon_0)\kappa_1^{(1)} + \kappa_2^{(1)}/2 \right), \tag{4.22}$$
$$\gamma_2 = \Gamma_R \left(\kappa_2^{(1)}/2 + f_R(\varepsilon_0)\kappa_2^{(1)}/2 \right),$$
$$\gamma_3 = \Gamma_L \left((1 - f_L(\varepsilon_0))\kappa_2^{(1)} + \kappa_1^{(1)}\kappa_2^{(2)} \right),$$
$$\gamma_4 = \Gamma_R \left(\kappa_2^{(1)} + (1 - f_R(\varepsilon_0))\kappa_1^{(1)}\kappa_1^{(2)} \right),$$
$$\gamma_5 = \Gamma_L \left((1 - f_L(\varepsilon_0))\kappa_2^{(1)} + \kappa_1^{(1)}/2 \right),$$
$$\gamma_6 = \Gamma_R \left(\kappa_2^{(1)} + (1 - f_R(\varepsilon_0))\kappa_1^{(1)}/2 \right),$$
$$\alpha = (\varepsilon_0 - \varepsilon_u)\kappa_2^{(1)} + (\varepsilon_u - \varepsilon_0)\frac{\kappa_1^{(1)}}{2}. \tag{4.23}$$

Where the κ's are given by

$$\kappa_1^{(1)} = \frac{1}{2}\left(1 + erf(\sqrt{4\lambda_1/\gamma_1})\right), \;\; \kappa_2^{(1)} = 1 - \kappa_1^{(1)} \text{ and } \kappa_1^{(2)} = \frac{1}{2}\left(1 + erf(\sqrt{4\lambda_2/\gamma_2})\right), \;\; \kappa_2^{(2)} = 1 - \kappa_2^{(2)}. \tag{4.24}$$

Here the κ's have the usual interpretation, we have introduced a superscript (1) and (2) to distinguish between the classical detector (1) and the detector causing back-action (2). $\kappa_1^{(1)}$ is the probability of the first detector to give the correct result, $\kappa_2^{(1)} = 1 - \kappa_1^{(1)}$ then gives probability to get wrong result, the same holds for $\kappa^{(2)}$.

The steady-state solution for this system can then be obtained and is given by

$$\rho_{00} = \frac{1}{\Omega}\left(\gamma_3\gamma_4\left(\alpha^2 + \omega^2\right) + 2g^2\omega\left(\gamma_3 + \gamma_4\right)\right), \tag{4.25}$$

$$\rho_{LL} = \frac{1}{\Omega}\left(\gamma_1\gamma_4\left(\alpha^2 + \omega^2\right) + 2g^2\omega\left(\gamma_1 + \gamma_2\right)\right),$$

$$\rho_{RR} = \frac{1}{\Omega}\left(\gamma_2\gamma_3\left(\alpha^2 + \omega^2\right) + 2g^2\omega\left(\gamma_1 + \gamma_2\right)\right),$$

$$\rho_{LR} = \frac{g}{\Omega}(\gamma_1\gamma_4 - \gamma_3\gamma_2)\left(\alpha + i\omega\right),$$

$$\rho_{RL} = \rho_{LR}^*.$$

With normalization factor given by

$$\Omega = \left(\alpha^2 + \omega^2\right)(\gamma_3\gamma_4 + \gamma_1\gamma_4 + \gamma_2\gamma_3) + 2g^2\omega\left(2(\gamma_1 + \gamma_2) + \gamma_3 + \gamma_4\right), \tag{4.26}$$

and where ω is given by

$$\omega = \frac{\gamma_5 + \gamma_6}{2} + 2\lambda_2. \tag{4.27}$$

Introducing the appropriate counting field, the current into the right reservoir is found to be given by

$$I = \frac{2g^2\omega}{\Omega}\left(\gamma_1\gamma_4 - \gamma_2\gamma_3\right). \tag{4.28}$$

Similarly, the second cummulant (fluctuations) is found to be

$$\Delta I = \frac{2\omega g^2\left(\gamma_2\gamma_3+\gamma_4\gamma_1\right)}{\Omega} - 2I^2\left(\frac{\mho}{\Omega}-\frac{1}{\omega}\right), \tag{4.29}$$

where

$$\mho = \left((\alpha^2+\omega^2)(\gamma_1+\gamma_2+\gamma_3+\gamma_4)+2g^2(2(\gamma_1+\gamma_2+\omega)+\gamma_3+\gamma_4)+2\omega(\gamma_1\gamma_4+\gamma_2\gamma_3+\gamma_3\gamma_4)\right). \tag{4.30}$$

Relative fluctuations are found by

$$\frac{\Delta I}{I} = \frac{\gamma_2\gamma_3+\gamma_1\gamma_4}{\gamma_1\gamma_4-\gamma_2\gamma_3} - 2I\left(\frac{\mho}{\Omega}-\frac{1}{\omega}\right). \tag{4.31}$$

For this system we will mainly consider the first cummulant (current) and leave only this analytical result for the second cummulant for the interested reader.

4.3.1 Sanity check - Overall Transport

We now perform a quick sanity check of the obtained results in order to validate that they agree with what is considered as minimally consistent, i.e that the transport conserves the number of electrons.

Let's look at the part of our system matrix corresponding to the classical transport

$$\begin{pmatrix} -\gamma_1-\gamma_2 & \gamma_3 & \gamma_4 \\ \gamma_1 & -\gamma_3 & 0 \\ \gamma_2 & 0 & -\gamma_4 \end{pmatrix}. \tag{4.32}$$

In order for the obtained result to be minimally consistent the total transport into the right reservoir must equal the total transport out from the left reservoir. The transports channels of interest are shown in figure 4.8 below.

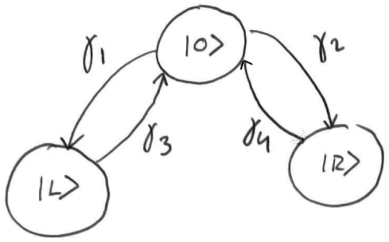

Figure 4.8: Classical transport channels in the double dot model.

Introducing the appropriate counting fields, the total current from the left reservoir into the system (I_1) and the total current going into the right reservoir (I_2) can be written as

$$I_1 = \gamma_1\rho_{00} - \gamma_3\rho_{LL} \quad I_2 = \gamma_4\rho_{RR} - \gamma_2\rho_{00}. \tag{4.33}$$

The consistency condition then becomes $I_1 = I_2$ or equally $I_1 - I_2 = 0$ which gives

$$I_1 = \frac{1}{\Omega}(\cancel{\gamma_1\gamma_3\gamma_4(\alpha^2+\omega^2)} + 2g^2\omega(\cancel{\gamma_1\gamma_3}+\gamma_1\gamma_4) - \cancel{\gamma_1\gamma_3\gamma_4(\alpha^2+\omega^2)} - 2g^2\omega(\gamma_1\gamma_3+\gamma_2\gamma_3) - 2g^2\omega(\cancel{\gamma_1\gamma_3}+\gamma_2\gamma_3)). \tag{4.34}$$

$$I_2 = \frac{1}{\Omega}\left(\cancel{\gamma_4\gamma_2\gamma_3}(\alpha^2+\omega^2) + 2g^2\omega(\gamma_1\gamma_4+\cancel{\gamma_2\gamma_4}) - \cancel{\gamma_2\gamma_3\gamma_4}(\alpha^2+\omega^2) - 2g^2\omega(\gamma_2\gamma_3+\cancel{\gamma_2\gamma_4})\right). \tag{4.35}$$

Which then gives

$$I_1 - I_2 = \frac{2g^2\omega}{\Omega}\left(\gamma_1\gamma_4-\gamma_2\gamma_3-\gamma_1\gamma_4+\gamma_2\gamma_3\right) = 0. \tag{4.36}$$

The overall transport is therefore consistent with $I_1 = I_2$.

4.3.2 More sanity checks - No control

Another consistency check of interest is to set the separation of the energy levels in the feedback scheme to zero i.e set $\varepsilon_0 = \varepsilon_L = \varepsilon_R = 0$. In this case the effect of feedback should vanish since the controller is no longer able to shift the levels depending on the state of the detector measurements. It is then expected that in the small $\lambda = \lambda_1 = \lambda_2$ regime to observe a current flow whose direction is only determined by difference in chemical potential $\Delta\mu$. However, since measurements are are still performed (but the controller is not able to act on the result) one expects the current to go towards zero for increasing λ since strong measurement should kill the coherence between the two quantum dots of the system and hence stop a current from flowing.

From the model we obtain the following result

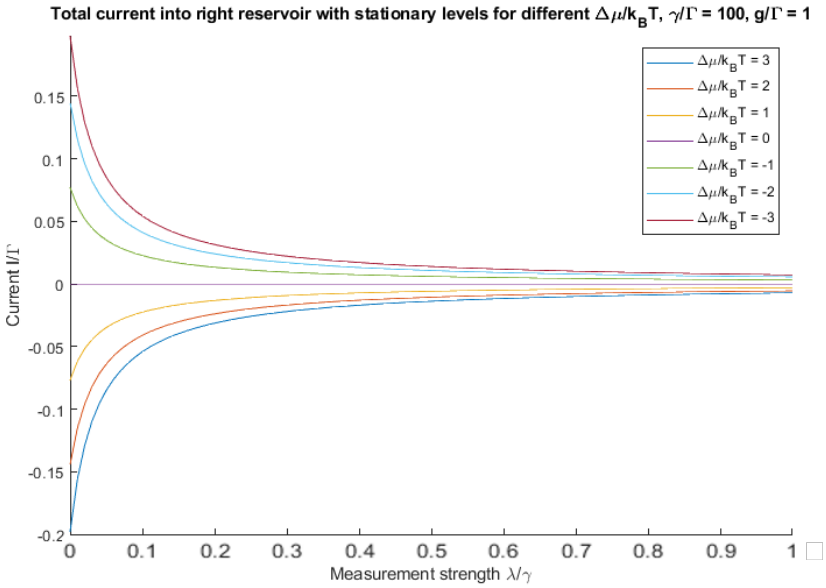

Figure 4.9: Total current into right reservoir for different values of $\Delta\mu$ when energy levels in the system are fixed. The results fits with what is expected, i.e. the direction of the current follows the gradient of the chemical potential when the energy levels are kept stationary at ε_0, here $\lambda = \lambda_1 = \lambda_2$ and $\gamma = \gamma_1 = \gamma_2$.

From figure 4.9 above it is noted that the model reproduces the expected result, i.e when the levels are kept stationary the current trough the system is determined by $\Delta\mu$. When the chemical potential of the left reservoir is higher than the right one ($\mu_r - \mu_l < 0 \implies \Delta\mu < 0$) there is a net flow from the left reservoir into the right one as dictated by thermodynamics, and the inverse process happens when $\Delta\mu > 0$ as expected. For $\Delta\mu = 0$ the current is identically zero irregardless of λ as is expected since there is no preferred direction for the current in this symmetric configuration. It is also noted that the expected effect of the measurement i.e to limit the current through decoherence for large measurement strengths are also reproduced. There is a clear trend of diminishing current for larger measurement strengths. This validity check therefore also contribute to the validity of the obtained results.

4.3.3 Ideal D_1 detector limit

Since it was seen above that the back-action for the D_1 measurement (which tells the controller whether or not there is an electron in the system or not) vanishes and hence does not cause any dechoerence of the system it might be justified to consider the limit where this detector gives perfect measurement outcome, i.e when λ_1 is arbitrarily large, even though this is formally outside of the region where the S.O.T approach is valid. The reasoning is due to the observation that for the classical system considered previously, there was no noticeable discrepancy between the

S.O.T and the exact numerical solution even for large λ/γ, since the classical measurement does not influence the dynamics of the system one expects the same to hold for this model. Hence, performing this limit putting $\kappa_1^{(1)} = 1$ and $\kappa_2^{(1)} = 0$ we obtain the following results

$$\begin{aligned}
\gamma_1 &= \Gamma_L f_L(\varepsilon_0), \\
\gamma_2 &= 0, \\
\gamma_3 &= \Gamma_L \kappa_2^{(2)}, \\
\gamma_4 &= \Gamma_R (1 - f_R(\varepsilon_0)) \kappa_1^{(2)}, \\
\gamma_5 &= \Gamma_L/2, \\
\gamma_6 &= \Gamma_R (1 - f_R(\varepsilon_0))/2, \\
\alpha &= (\varepsilon_u - \varepsilon_0)/2.
\end{aligned} \tag{4.37}$$

It is noted that in with these two approximations, the system is very close to the ideal transport operation. This approximation have completely closed the classical transport channel between $|0\rangle \to |R\rangle$. Hence, there is no back-current from the right reservoir into the system. There is one back-current that remains through the transport channel given by γ_3 however this one is governed by the accuracy of the D_2 detector.

4.3.4 Some other limits of interest

Note that $\Omega \propto g^2$ for large g and $\Omega \propto \omega^2$ for large ω. Here some limits that may be off interest are investigated.

Large ω (λ)

First consider the large ω limit of I. Then $I \propto \omega/\omega^2 \to 0$, the large ω limit is the large λ limit, i.e. large strength of the measurement. It is therefore noted that for strong measurements the current through the double dot tends to zero. This is expected for this quantum system and is referred to as the Zeno effect. In this quantum system there needs to be a coherence build-up between the levels in order for the transition $|L\rangle \to |R\rangle$ to occur. With sufficiently large measurement strength this coherence build-up is suppressed. The Zeno effect is often discussed in the context of using measurement to suppress transitions i.e forcing the system to be in the observed state [25], the observed effect is completely analogous to this situation. We also note that the coherence part of the density matrix vanishes in the the large λ limit which is expected.

Large g

Let's consider the limit of large g, i.e when there is a very strong coupling between the levels. In this limit the current reduces to

$$I = \frac{\gamma_1\gamma_4 - \gamma_2\gamma_3}{2\gamma_1 + 2\gamma_2 + \gamma_3 + \gamma_4}. \tag{4.38}$$

This result is quite interesting because it closely resembles the result obtained for the classical system in Chapter 3 (See equation 3.27). Hence, one might be able to argue that the large coupling factor limit is related to a transition between the quantum and classical regime of the system. It is also noted that in the limit of large coupling factor g the coherence part of ρ also vanishes.

4.3.5 Power production considerations

For the double dot system the power production is considered under the assumption of ideal energy level placings i.e $f_{L/R}(\varepsilon_d) = 1$ and $f_{L/R}(\varepsilon_u) = 0$, as well as under the assumption of an ideal D_1 detector meaning $\kappa_1^{(1)} = 1$ and

$\kappa_2^{(1)} = 0$. Under these assumptions the different currents of the system becomes manageable and it is possible to investigate regions where the system behaves as a Maxwell demon. Under these assumptions the classical transports of the system reduces three currents I_1, I_2, I_3 as shown in figure 4.10 below

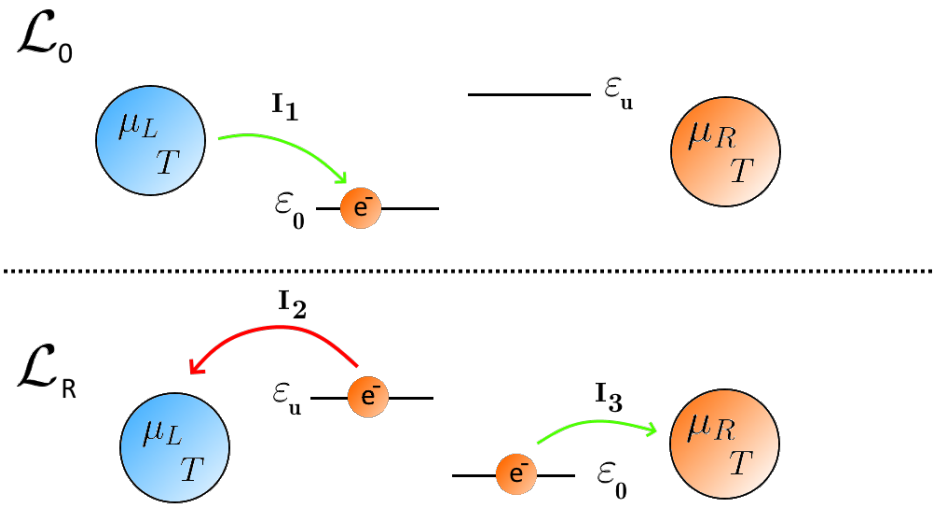

Figure 4.10: Remaining currents under idealized assumption, during $\mathcal{L}_0$ current can only enter from the left, during $\mathcal{L}_L$ no transport occurs between the reservoirs (not shown in figure), during $\mathcal{L}_R$ electrons can either be moved into the right reservoir or back into the left reservoir due to feedback error.

For these conditions $I_1 = I_2 + I_3$ holds. In terms of power production only I_3 is a process where $W_{\text{levels}} = 0$ while every electron leaving through I_2 costs $W_{\text{levels}} = \varepsilon_u - \varepsilon_0 = \Delta\varepsilon/2$, i.e. work must be put into the system. Introducing appropriate counting fields for the currents and weighing them by their energy cost/production the following expression is obtained

$$W_{\text{chemical}} - W_{\text{levels}} = \Delta\mu I_3 - \frac{\Delta\varepsilon}{2} I_2 = \frac{2g^2\omega\gamma_1\gamma_4\Delta\mu}{\Omega} - \frac{\gamma_3\Delta\varepsilon}{2\Omega}\left(\gamma_1\gamma_4(\alpha^2+\omega^2) - 2g^2\omega\gamma_1\right). \tag{4.39}$$

In order for the feedback to generate more power by moving electrons against the difference in chemical potential then is consumed in the feedback error of moving the electrons back into the left reservoir at ε_u the following must hold $W_{\text{chemical}} - W_{\text{levels}} > 0$. Under normal conditions the I_2 term turns out to be quite large compared to the I_3 term. However, since the I_2 term is $\propto \gamma_3 \propto \kappa_2^{(2)}$ this term should vanish as λ_2 increases. Note that increased λ_2 generally leads to diminished current through the system. Hence, there seems to be a trade-off in λ_2 and other parameters such as g instead becomes important in deciding where positive power generation occurs.

4.4 Analytical Results

In the following section we consider the current into the right reservoir as a function of $\Delta\mu$ under the assumption $f_{L/R}(\varepsilon_d) = 1$ and $f_{L/R}(\varepsilon_u) = 0$. We set $\varepsilon_u - \varepsilon_d = 20k_bT$, $\gamma/\Gamma = 100$.

First a non-ideal classical detector is considered, we set $\gamma = \gamma_1 = \gamma_2$ and $\lambda = \lambda_1 = \lambda_2$. For the double dot system there are some clear differences in the behaviour of the current when compared to the classical system. For the non-ideal case (figures 4.11a-4.11c) a clear maximum in the current into the right reservoir is observed. This maximum is moved to larger values of λ/γ for increasing g but the sharpness of the peak is also strongly influenced by the value of $\Delta\mu$ and seem to become less sharp for larger biases. For this system the value of λ also starts to become important and it is clearly seen that the current is suppressed for increasing values of λ. However, this suppression is not especially strong and seems to be able to be counteracted by quite modest values of g/Γ.

What is more interesting is that the current into the right reservoir does not go to zero or is necessarily negative for $\Delta\mu \geq 0$ when $\lambda/\gamma = 0$ i.e when the feedback protocol is applied randomly. With figure 4.9 in mind this current must come from the way that the feedback protocol is setup. We argue that it is due to an asymmetry in the way that the feedback is setup. Looking at the operation cycle in detector space (figure 4.7) it is noted that twice the area of the detector space is reserved for $\mathcal{L}_0$ meaning that if feedback is applied randomly the controller is twice as likely to apply $\mathcal{L}_0$ compared to $\mathcal{L}_L$ and $\mathcal{L}_R$. If it by chance happens to be the case that the right state is occupied it is therefore more likely for the system to apply $\mathcal{L}_0$ hence lifting the electron to ε_u at which point it would instantly move into the right reservoir. It is therefore due to this asymmetry, the process that can only put electrons into the right reservoir is twice as likely to be applied then processes that could remove electrons from the right reservoir. That there is a current into the right reservoir even if feedback is applied randomly. It is seen that this process only happens if $\Delta\mu$ is not to large, at some point the voltage bias is large enough to be able to resist this asymmetry.

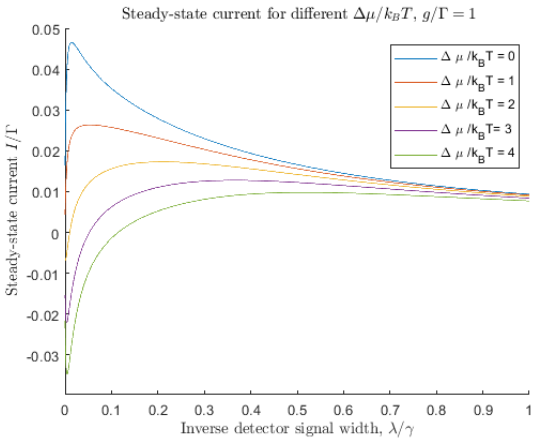

(a)

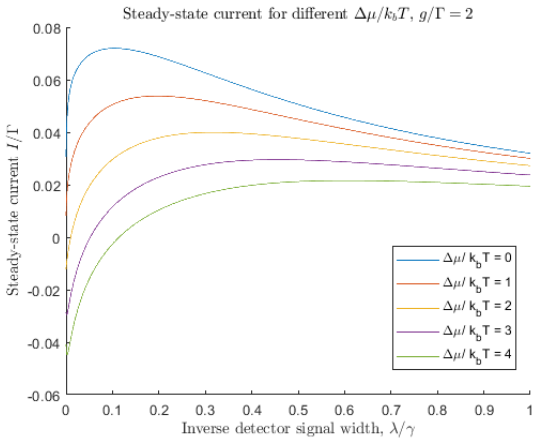

(b)

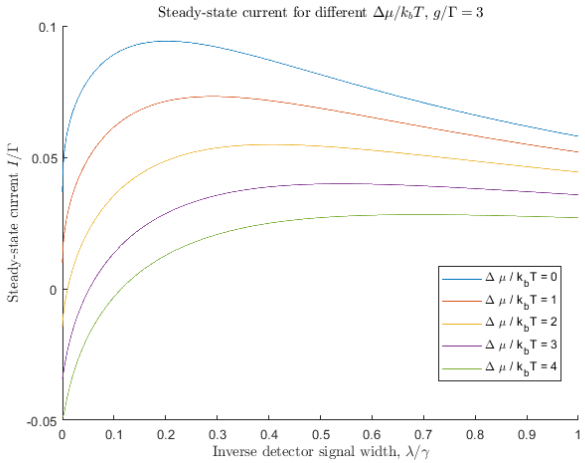

(c)

Figure 4.11: Current into right reservoir for different $\Delta\mu$ (in units of k_bT) and g (in units of Γ). Non-ideal classical detector, $\gamma = \gamma_1 = \gamma_2$ and $\lambda = \lambda_1 = \lambda_2$.

We now consider an ideal classical detector i.e $k_1^{(1)} = 1$ and $k_2^{(1)} = 0$. Furthermore, we have $\gamma = \gamma_2$ and $\lambda = \lambda_2$. For the ideal classical detector case (figures 4.12a-4.12c) very similar behaviour compared to the non-ideal case is observed. In this ideal case the classical detector always returns the correct value, meaning that the controller is certain whether or not there is an electron present in the system. It is not certain, however, if the electron is in the left or right state since this is determined by the second detector which contributes back-action of the system.

Overall the current for the ideal case is systematically larger then for the non-ideal case as is expected. It is also observed that the current in this limit is always positive hence a perfect classical detector is enough in order to pump electrons from the left reservoir into the right reservoir for larger values of $\Delta\mu/k_BT$ then the non-ideal case manages.

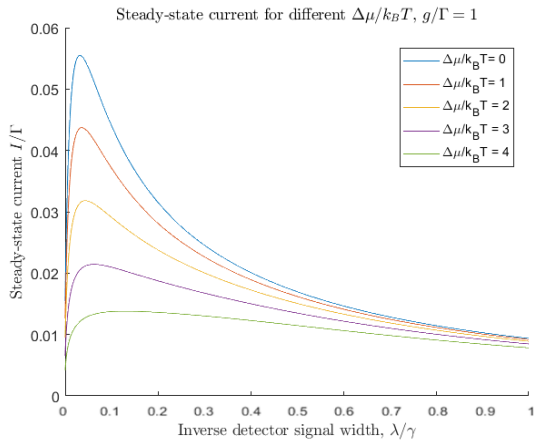

(a)

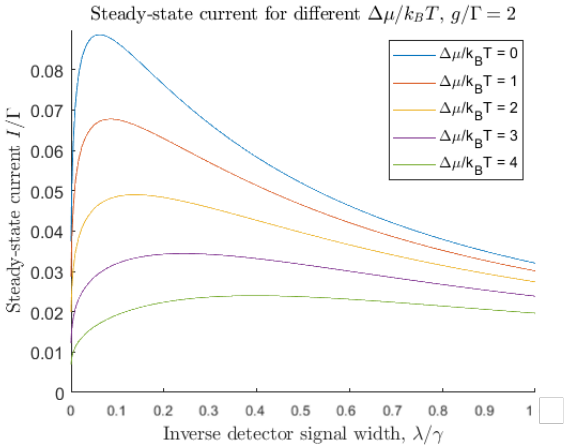

(b)

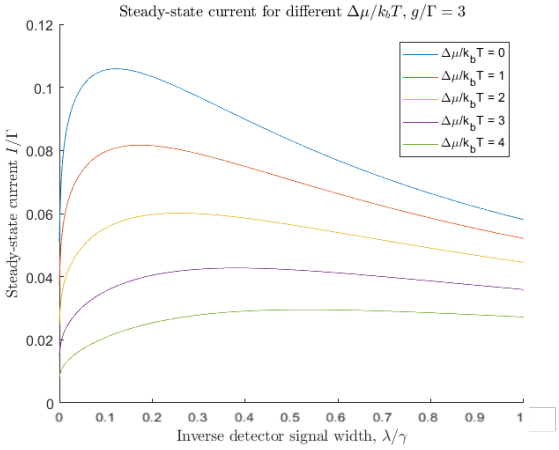

(c)

Figure 4.12: Current into right reservoir for different $\Delta\mu$ (in units of k_bT) and g (in units of Γ) for a perfect classical detector, $\gamma = \gamma_2$ and $\lambda = \lambda_2$.

4.5 Numerics

For the numerics of the double dot system a hybrid approach was used, the full 2 detector Fokker-Planck equation was deemed too computationally expensive since that for even small numbers of polynomials in the expansion the system matrix becomes too large. Assuming that n number of polynomials are used in the expansion of the density matrix, the final system equation matrix have dimensions of $5n^2 \times 5n^2$. The method for finding the solution turns out to have very poor scaling ($\mathcal{O}(m^3)$ where m is the number of rows (or columns) in the system matrix). This then becomes too computationally expensive even for quite modest number of polynomials where convergence is not guaranteed.

In order to simplify the problem a different approach was instead investigated, utilizing that the D_1 detector does not cause any dephasing of the system and hence that this detector should in principle behave as the detector considered for the classical system where the separation of timescales approximation agreed very well with the full numerical solution even for $\gamma \approx \lambda$.

For the numerical approach it is therefore assumed that the D_1 detector is given by the separation of timescales approximation and that the ideal limit considered in section 4.3.3 is applicable, this reduces the problem to a one-dimensional Fokker-Planck equation that can then readily be solved. More details about the numerics can be found in the appendix (6.2.2).

4.6 Numerics Results

We begin by considering the steady state detector distribution function. The following results are for symmetric tunneling $\Gamma_L = \Gamma_R = \Gamma$, $\Delta\mu = 0$, $\varepsilon_u - \varepsilon_d = 20k_BT$. Fixing g and $\gamma = \gamma_2$ such that $\gamma/g = 100$. We investigate the detector distribution function for different Γ/γ and λ_2/γ. 400 polynomials was used in the expansion to reach convergence. For the detector distribution function we note that the agreement between the separation of timescales approximation and the full (hybrid) numerics is remarkably strong (as can be seen in figures 4.13a to 4.15c). This agreement also holds for smaller values of γ/g (when coupling timescale approaches detector timescale) such as $\gamma/g = 20, 10, 1$. The reasons why the agreement is as good as it seems is probably due to the fact that the $|L\rangle$ state is dominating the process, for example in figure 4.13c a small component of the detector distribution can be seen coming from the $|R\rangle$ state (since that state gives a signal around $D = 1$). The numerics seems to resolve this abit better than the analytical approximation. In most other cases either the $|0\rangle$ or $|L\rangle$ state is dominating the process and it seems that in these cases the analytical approximation is exceptionally accurate when it comes to the detector distribution function.

From the plots of the detector distribution the effect of increasing λ is clearly seen, the detector distribution starts out quite symmetric around $D = 0$ but moves closer to $D = -1$ as λ is increased, this is likely due to the fact that increasing λ suppresses the coherent coupling making it harder for an electron in the $|L\rangle$ to move into the $|R\rangle$ state, since the electron then sits in $|L\rangle$ for a majority of the time this signal is dominating the detector distribution in steady state. Increasing the tunneling rate Γ seem to have similar effect, i.e. the $|L\rangle$ state is more rapidly filled but the coupling g acts as a bottleneck in the system and the system then stays in $|L\rangle$ most of the time (As soon as $|R\rangle$ is detected it should also quite quickly move out into the right reservoir).

$\Gamma/\gamma = 0.01$

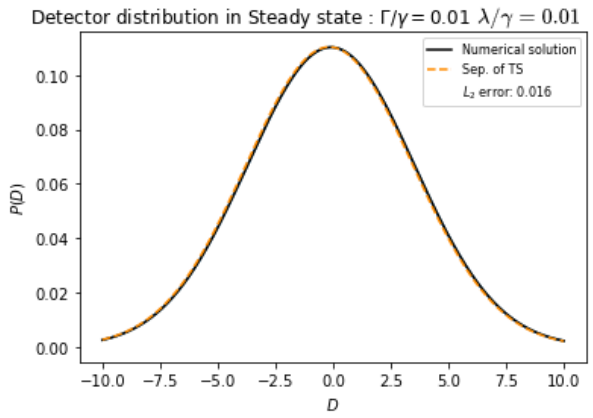

(a)

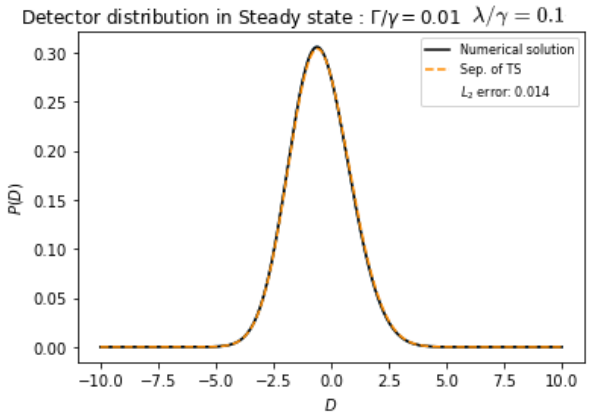

(b)

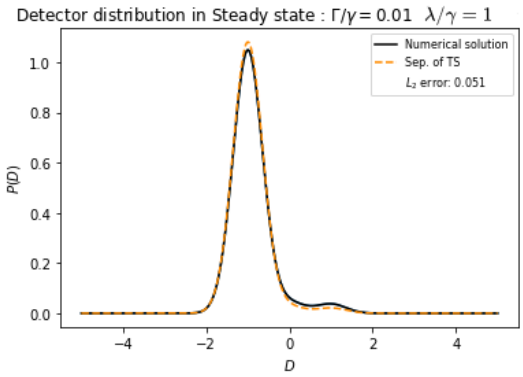

(c)

Figure 4.13: Detector distribution function at steady state for $\Gamma/\gamma = 0.01$, $\gamma/g = 100$, for different values of λ/γ .

$\Gamma/\gamma = 0.1$

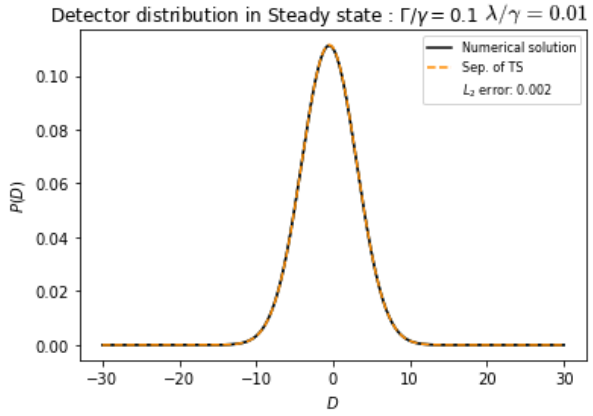

(a)

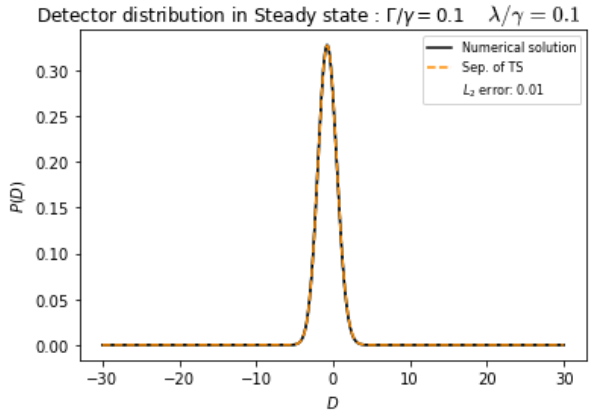

(b)

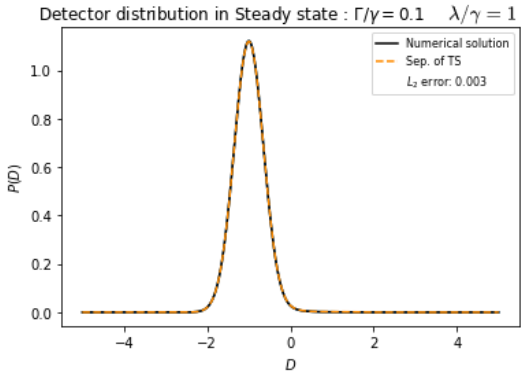

(c)

Figure 4.14: Detector distribution function at steady state for $\Gamma/\gamma = 0.1$, $\gamma/g = 100$, for different values of λ/γ.

$\Gamma/\gamma = 1$

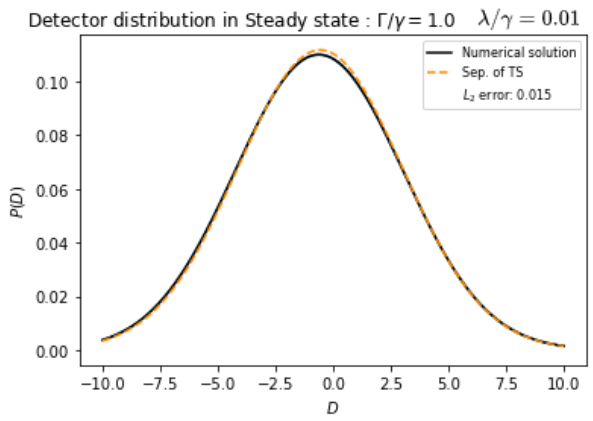

(a)

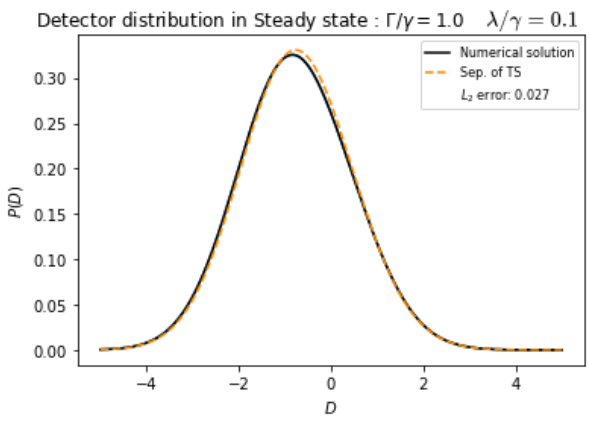

(b)

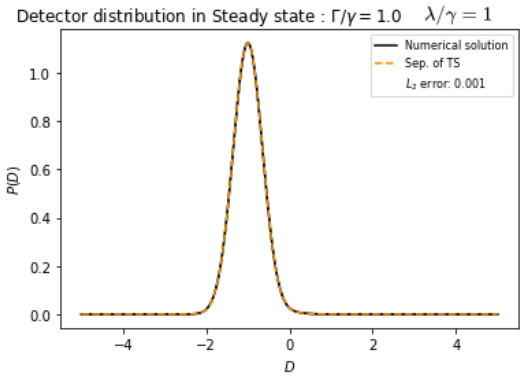

(c)

Figure 4.15: Detector distribution function at steady state for $\Gamma/\gamma = 1$, $\gamma/g = 100$, for different values of λ/γ.

We now consider the power production for the idealized system. From the power production plots (figures 4.16a - 4.16c) it is seen that there are regions where the net power production is positive and where the system therefore behaves as a Maxwell demon. For small values of λ/γ the error current is dominating the process meaning that the system acts as an electron pump were energy is put into the system by the levels. However, as discussed above for sufficiently large λ/γ, this error process is suppressed to such an extent that the remaining wanted current through the system takes over. It is noted that in order for the wanted current to be able to dominate, the value of g/γ needs to be sufficiently large otherwise the necessary dephasing rate λ needed to suppress the error current will also suppress the current through the system into the right reservoir. Once g/γ is large enough to keep some coherence at larger values of λ/γ where the error current has been suppressed the power production seems to plateau somewhat (but goes to zero for larger values of λ/γ for fixed γ), at this point the maximum value of the power production seems to be decided upon by the applied chemical potential bias.

It is also clearly seen from the current plots that there is a disagreement between the numerically calculated current and the analytically calculated current once the error current has been suppressed. Since the wanted current is related to the $|R\rangle$ state, this also seems to imply that the numerics resolves the $|R\rangle$ state somewhat better but since this state is not populated as much as $|0\rangle$ and $|L\rangle$ during the process this is not clearly seen when considering only the total detector distribution function.

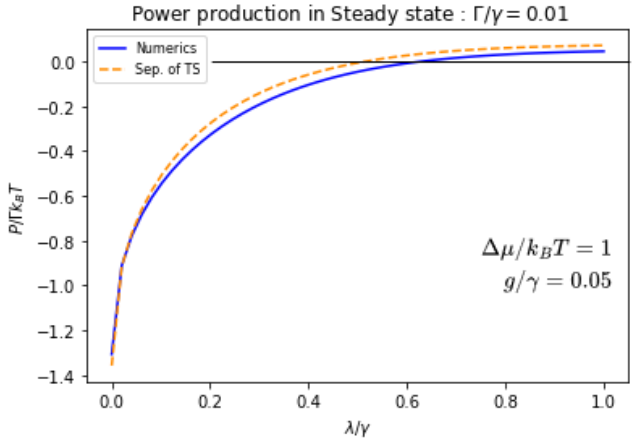

(a)

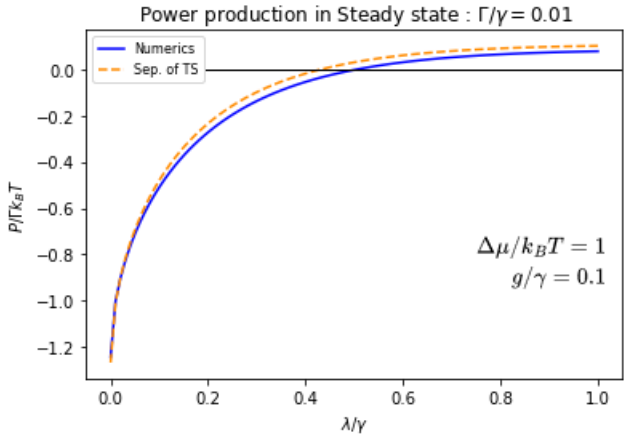

(b)

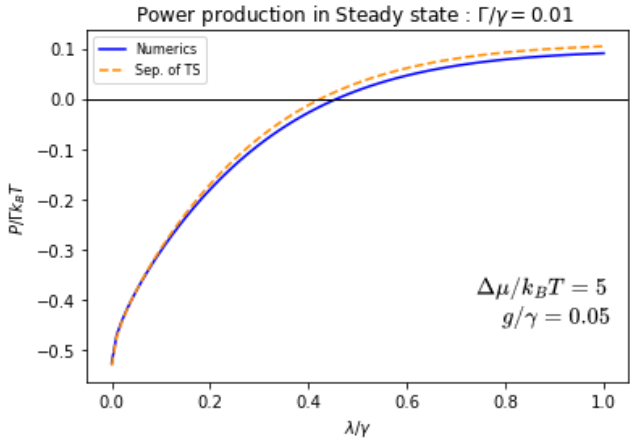

(c)

Figure 4.16: Power production for double dot system in the idealised situation for some different values of g/γ and $\Delta\mu/k_BT$, as a function of λ/γ. Black line indicates transition when system transitions from negative to positive power production showing when the system becomes a Maxwell demon.

Chapter 5

Conclusions & Outlook

This thesis have treated the novel formalism for describing feedback for quantum system described in [11]. The formalism was applied to two different test systems, one classical and one quantum. The transport properties for the systems were investigated both analytically and numerically using full counting statistics. It was shown that both systems could be operated as information engines using the proposed feedback schemes.

For the classical system the analytical results and the full numerics agreed very well in the regions where the separation of timescales approximation is supposed to hold, validating the legitimacy of this approximate approach. As the system timescale became comparable with the detector timescale larger and larger discrepancies were observed. It was also noted that the dephasing caused by the measurement did not influence the dynamics of the system and that the detector accuracy could be made arbitrarily good without affecting the dynamics of the system. Hence, the seperation of timescales approximation seemed to hold for regions outside where it formally should be accurate for classical systems. It was also observed that while the actual achievable current through the system was in principle determined by the value of Γ at optimal operation. The ratio between the first and second cummulant was found to be bounded from below by $1/2$ meaning that the fluctuations of the transport could not be made arbitrarily small by the feedback process. For sufficiently large values of λ/γ (determined by $\Delta\mu/k_BT$) it was shown that the system acts as a Maxwell demon.

For the quantum double dot system using the proposed feedback scheme it was realized that two separate detectors were needed in order to avoid performing erroneous feedback operations. It was shown that it was possible to choose these detectors as one detector measuring the total charge of the system which did not cause any back-action on the system and another detector which is able to resolve whether or not the left or right states are occupied. Using this double detector approach the analytical results implied that the system acts as an electron pump when applying feedback with large errors (low values of λ/γ) seemingly being able to transport electrons against a chemical potential bias without trading information. However, it was argued that this apparent transport was due to an asymmetry in the way that the feedback process was setup and that any energy gained was necessarily compensated by energy put in through the movement of the energy levels.

In the limit of an ideal classical detector is was possible to compare the analytical results with a full numerical solution. The results were shown to agree very well with the full numerics. However, the full numerical solution gave slightly different occupation of the $|R\rangle$ state which the analytical solution seemed to over-estimate. Finally it was shown that as the accuracy of the second detector was increased there exists a region where it is possible to operate the double dot system as an information engine for sufficiently large values of the coupling constant g between the two dots.

For future studies of the double dot system using this formalism it would be interesting to have some experimental input in order to be able to verify the validity of the formalism considered. Such studies are scheduled to be performed at Nanolund in the latter part of 2022. These experimental studies will provide invaluable input for further theoretical studies. Similarly, a Monte-Carlo style investigation of the double dot system with the proposed feedback could be performed in order to test the validity of the results obtained in this thesis, this could also be used in order to investigate to what extent erroneous feedback is avoided by the use of two detectors and maybe even find limits where one detector turns out to be sufficient.

It would also be interesting to consider other feedback schemes in order to investigate whether or not the proposed feedback scheme has maximal efficiency or if there are other feedback schemes that utilizes the coherency of the system in order to gain an advantage. Finally it would be necessary to find a more efficient approach for solving the Quantum-Fokker Planck Master equation numerically for a 2D detector space. Improvements could be made in the choice of basis functions or more efficient numerical methods could be investigated. If it would be possible to parallelize the computations in an efficient manner a powerful cluster could perhaps be used in order to increase the accuracy of the obtained numerical solutions as well as make it possible to investigate even more complicated systems with more sophisticated feedback schemes.

Similarly for the classical model for the S.E.T system it would interesting to investigate whether it is possible to find an optimal feedback scheme for maximizing power production and whether or not different feedback schemes are able to decrease the fluctuations in the transport further. This system would also benefit from a Monte-Carlo investigation in order to validate the obtained results as well as the overall validity of the formalism.

Chapter 6

Appendix

6.1 Proof of useful expressions

Consider a density matrix ρ and some observable $\hat{A}$ then we can derive some useful identities. Since the eigenstates of an observable span the Hilbert space we can express the density matrix in terms of the eigenstates of $\hat{A}$. For simplicity we assume that $\hat{A}$ has a continuous spectrum (makes no difference).

$$\rho = \iint dada' \left|a\right\rangle\!\left\langle a\right| \rho \left|a'\right\rangle\!\left\langle a'\right| = \iint dada' \rho_{a,a'} \left|a\right\rangle\!\left\langle a'\right| \tag{6.1}$$

Where we have inserted the identity operator ($\int da \left|a\right\rangle\!\left\langle a\right| = \mathbb{1}$) twice. We then derive the following identities

6.1.1 Identity 1

$$\hat{A}\rho\hat{A} - \frac{1}{2}\{\hat{A}^2, \rho\} = \hat{A}\rho\hat{A} - \frac{1}{2}\left(\hat{A}^2\rho + \rho\hat{A}^2\right) = \iint dada' \rho_{a,a'} \left[\hat{A}\left|a\right\rangle\!\left\langle a'\right|\hat{A} - \frac{1}{2}\left(\hat{A}^2\left|a\right\rangle\!\left\langle a'\right| + \left|a\right\rangle\!\left\langle a'\right|\hat{A}^2\right)\right] \tag{6.2}$$

$$= \iint dada' \rho_{a,a'} \left|a\right\rangle\!\left\langle a'\right| \left[aa' - \frac{1}{2}\left(a^2 + a'^2\right)\right] \tag{6.3}$$

6.1.2 Identity 2

$$\{\hat{A}, \rho\} = \hat{A}\rho + \rho\hat{A} = \iint dada' \rho_{a,a'} \hat{A}\left|a\right\rangle\!\left\langle a'\right| + \left|a\right\rangle\!\left\langle a'\right|\hat{A} = \iint dada' \rho_{a,a'} \left|a\right\rangle\!\left\langle a'\right| (a + a') \tag{6.4}$$

6.2 Details of Numerics

Code for the numerics can be found at `https://github.com/Danefantom/ExjobbNumerics.git`

6.2.1 SET system

For the classical system the following parametrization of the density matrix was chosen as

$$\rho = \begin{pmatrix} a & b \\ c & d \end{pmatrix} \rightarrow \begin{pmatrix} a & d & b & c \end{pmatrix}^T.$$

Since the populations were decoupled from the coherences we worked with only (a, d). The following expansion was then used

$$\rho(D) = \sum_n \frac{H_{e_n}^{[\sigma]}(D)}{\sqrt{\sigma^n n!}} \frac{e^{-D^2/2\sigma}}{\sqrt{2\pi\sigma}} \begin{pmatrix} a_n & d_n \end{pmatrix}^T .$$

This expansion was then put into Eq.(2.39). A homogeneous system of equations was then obtained by multiplying the equation with the $H_{e_k}^{[\sigma]}(D)$ components in the expansion and integrating over D. In this particular implementation the coefficient vector was split into the a part and the d part and the system matrix was constructed accordingly

6.2.2 Quantum Double Dot

For the Double Dot system the parametrization of the density matrix was chosen as

$$\rho = \begin{pmatrix} a & 0 & 0 \\ 0 & b & c \\ 0 & c^* & d \end{pmatrix} \rightarrow \begin{pmatrix} a & b & d & \mathrm{Re}(c) & \mathrm{Im}(c) \end{pmatrix}^T .$$

For the Double Dot system the full 2D expansion of the density matrix turned out to be too computationally expensive. Instead a hybrid approach was used. It was assumed that the classical detector function was given by the separation of timescales solution. With this assumption the expansion used is given by

$$\rho(D_1, D_2) = \sum_n \frac{H_{e_n}^{[\sigma]}(D_2)}{\sqrt{\sigma^n n!}} \frac{e^{-D_2^2/2\sigma}}{\sqrt{2\pi\sigma}} \begin{pmatrix} G_{00}^{(1)}(D_1) a_n & G_{LL}^{(1)}(D_1) b_n & G_{RR}^{(1)}(D_1) d_n & G_{LR}^{(1)}(D_1)\,\mathrm{Re}(c_n) & G_{RL}^{(1)}(D_1)\,\mathrm{Im}(c_n) \end{pmatrix}^T .$$

The full version of Eq.(2.39) could then be integrated over D_1 giving the new equation

$$\dot{\rho}(D_2) = \int_{D_1} dD_1 \mathcal{L}(D_1, D_2)\rho(D_1, D_2) + \lambda_2 \mathcal{D}[\hat{\sigma_2}]\rho(t, D_2) - \gamma_2 \partial_{D_2} \frac{1}{2} \{\sigma_2 - D_2, \rho(t, D_2)\} + \frac{\gamma_2^2}{8\lambda_2} \partial_{D_2}^2 \rho(t, D_2).$$

This reduced equation could then readily be solved in steady-state using the same method as for the classical system.

Bibliography

[1] P.W. Shor. Algorithms for quantum computation: discrete logarithms and factoring. In *Proceedings 35th Annual Symposium on Foundations of Computer Science*, pages 124–134, 1994.

[2] Jing Zhang, Yu xi Liu, Re-Bing Wu, Kurt Jacobs, and Franco Nori. Quantum feedback: Theory, experiments, and applications. *Physics Reports*, 679:1–60, 2017.

[3] Goetsch, Tombesi, and Vitali. Effect of feedback on the decoherence of a schrödinger-cat state: A quantum trajectory description. *Physical review. A, Atomic, molecular, and optical physics*, 54 5:4519–4527, 1996.

[4] M. A. Castellanos-Beltran and K. W. Lehnert. Widely tunable parametric amplifier based on a superconducting quantum interference device array resonator. *Applied Physics Letters*, 91(8):083509, 2007.

[5] R. Vijay, C. Macklin, D. H. Slichter, S. J. Weber, K. W. Murch, R. Naik, A. N. Korotkov, and I. Siddiqi. Stabilizing rabi oscillations in a superconducting qubit using quantum feedback. *Nature*, 490(7418):77–80, Oct 2012.

[6] D. Ristè, C. C. Bultink, K. W. Lehnert, and L. DiCarlo. Feedback control of a solid-state qubit using high-fidelity projective measurement. *Phys. Rev. Lett.*, 109:240502, Dec 2012.

[7] Viacheslav Belavkin. Non-demolition measurement and control in quantum dynamical systems. In A. Blaquiere, S. Diner, and G. Lochak, editors, *Information Complexity and Control in Quantum Physics*, pages 311–329, Vienna, 1987. Springer Vienna.

[8] H. M. Wiseman. Quantum theory of continuous feedback. *Phys. Rev. A*, 49:2133–2150, Mar 1994.

[9] H. M. Wiseman and G. J. Milburn. Quantum theory of optical feedback via homodyne detection. *Phys. Rev. Lett.*, 70:548–551, Feb 1993.

[10] Vasco Cavina, Andrea Mari, Alberto Carlini, and Vittorio Giovannetti. Optimal thermodynamic control in open quantum systems. *Phys. Rev. A*, 98:012139, Jul 2018.

[11] Björn Annby-Andersson, Faraj Bakhshinezhad, Debankur Bhattacharyya, Guilherme De Sousa, Christopher Jarzynski, Peter Samuelsson, and Patrick P. Potts. Quantum fokker-planck master equation for continuous feedback control, 2021. arXiv:2110.09159.

[12] Leo Szilard. On the decrease of entropy in a thermodynamic system by the intervention of intelligent beings. *Behavioral Science*, 9(4):301–310, 1964.

[13] Cargill Gilston Knott. *Life and scientific work of Peter Guthrie Tait supplementing the two volumes of scientific papers published in 1898 and 1900.* Cambridge [Eng.] :University Press,. https://www.biodiversitylibrary.org/bibliography/17932.

[14] R. Landauer. Irreversibility and heat generation in the computing process. *IBM Journal of Research and Development*, 5(3):183–191, 1961.

[15] Antoine Bérut, Artak Arakelyan, Artyom Petrosyan, Sergio Ciliberto, Raoul Dillenschneider, and Eric Lutz. Experimental verification of landauer's principle linking information and thermodynamics. *Nature*, 483(7388):187–189, Mar 2012.

[16] Shoichi Toyabe, Takahiro Sagawa, Masahito Ueda, Eiro Muneyuki, and Masaki Sano. Experimental demonstration of information-to-energy conversion and validation of the generalized jarzynski equality. *Nature Physics*, 6(12):988–992, Dec 2010.

[17] U. Fano. Description of states in quantum mechanics by density matrix and operator techniques. *Rev. Mod. Phys.*, 29:74–93, Jan 1957.

[18] J. von Neumann. Wahrscheinlichkeitstheoretischer aufbau der quantenmechanik. *Nachrichten von der Gesellschaft der Wissenschaften zu Göttingen, Mathematisch-Physikalische Klasse*, 1927:245–272, 1927.

[19] Léon van Hove. Von neumann's contributions to quantum theory. *Bulletin of the American Mathematical Society*, 64:95–99, 1958.

[20] Michael A. Nielsen and Isaac L. Chuang. *Quantum Computation and Quantum Information: 10th Anniversary Edition*. Cambridge University Press, USA, 10th edition, 2011.

[21] J. J. Sakurai and Jim Napolitano. *Modern Quantum Mechanics*. Cambridge University Press, 2 edition, 2017.

[22] Daniel Manzano. A short introduction to the lindblad master equation. *AIP Advances*, 10(2):025106, 2020.

[23] Heinz-Peter Breuer and Francesco Petruccione. *The Theory of Open Quantum Systems*. Oxford University Press, Oxford, 2007.

[24] Dariusz Chruściński and Saverio Pascazio. A brief history of the gkls equation. *Open Systems & Information Dynamics*, 24(03):1740001, 2017.

[25] Adam Bednorz, Wolfgang Belzig, and Abraham Nitzan. Nonclassical time correlation functions in continuous quantum measurement. *New Journal of Physics*, 14(1):013009, jan 2012.

[26] Carlton M. Caves and G. J. Milburn. Quantum-mechanical model for continuous position measurements. *Phys. Rev. A*, 36:5543–5555, Dec 1987.

[27] A. Barchielli, L. Lanz, and G. M. Prosperi. A model for the macroscopic description and continual observations in quantum mechanics. *Il Nuovo Cimento B (1971-1996)*, 72(1):79–121, Nov 1982.

[28] Kurt Jacobs. *Quantum Measurement Theory and its Applications*. Cambridge University Press, 2014.

[29] Kurt Jacobs and Daniel A. Steck. A straightforward introduction to continuous quantum measurement. *Contemporary Physics*, 47(5):279–303, 2006.

[30] Taylor Lee Patti, Areeya Chantasri, Luis Pedro García-Pintos, Andrew N. Jordan, and Justin Dressel. Linear feedback stabilization of a dispersively monitored qubit. *Phys. Rev. A*, 96:022311, Aug 2017.

[31] C. W. Gardiner. *Handbook of stochastic methods for physics, chemistry and the natural sciences*, volume 13 of *Springer Series in Synergetics*. Springer-Verlag, Berlin, third edition, 2004.

[32] S. Shreve I. Karatzas. *Brownian Motion and Stochastic Calculus*. Springer, New York, 2th edition, 1998.

[33] Björn Annby-Andersson. Info as fuel project. *Personal notes*, mar 2021.

[34] Gernot Schaller. *Open Quantum Systems Far from Equilibrium*. Springer, Cham, Switzerland, 1th edition, 2014.

[35] K. F. Riley, M. P. Hobson, and S. J. Bence. *Mathematical Methods for Physics and Engineering: A Comprehensive Guide*. Cambridge University Press, 3 edition, 2006.

[36] Eric Jones, Travis Oliphant, Pearu Peterson, et al. SciPy: Open source scientific tools for Python, 2001–.

[37] Björn Annby-Andersson, Peter Samuelsson, Ville F. Maisi, and Patrick P. Potts. Maxwell's demon in a double quantum dot with continuous charge detection. *Phys. Rev. B*, 101:165404, Apr 2020.